Coordination Chemistry Reviews 532 (2025) 216523

Contents lists available at ScienceDirect

Coordination Chemistry Reviews

journal homepage: www.elsevier.com/locate/ccr

Contrast enhancement in medical imaging: At the crossroads of techniques and contrast agents – Improvements over the last decade

Camille Gosée [a,b], Cyril Cadiou [a,*], Juliette Moreau [a], Maité Callewaert [a], Christelle Kowandy [a], Céline Henoumont [b], Lionel Larbanoix [c], Sophie Laurent [b,c,**], Françoise Chuburu [a,*]

[a] University of Reims Champagne Ardenne, CNRS, ICMR UMR, 7312 Reims, France
[b] General, Organic and Biomedical Chemistry Unit, NMR and Molecular Imaging Laboratory, University of Mons, UMONS, B-7000 Mons, Belgium
[c] Center for Microscopy and Molecular Imaging, University of Mons, Rue Adrienne Bolland 8, B-6041 Charleroi, Belgium

ARTICLE INFO

Keywords:
Computed Tomography (CT)
Ultrasounds (US)
Magnetic Resonance Imaging (MRI)
Single Photon Emission Computed Tomography (SPECT)
Positron Emission Tomography (PET)
Optical Imaging (OI)
Photoacoustic Imaging (PAI)
Contrast agents - MRI/PAI probes

ABSTRACT

Early detection and diagnosis of pathologies is an essential part of clinical practice. This continually drives improvements in imaging modalities and contrast agents. The challenge is always to obtain the most accurate images possible of lesions, but also to detect tissue microstructures or metabolic events. This means combining resolution and sensitivity with deep-tissue imaging. Here, we review examples of contrast agents used in the various biomedical imaging modalities currently in use (CT, US, MRI, SPECT, PET, Fluorescence). We will then take a closer look at photoacoustic imaging (PAI), because of its intrinsic resolution and sensitivity. The review is structured as follows: first, the principle of each technique is discussed, followed by a description of the characteristics that the dedicated contrast agents must meet. Third, recent examples of molecular and nanoparticulate contrast agents will be described. Finally, a special section will be devoted to bimodal contrast agents combining MRI and PAI imaging, showing that it is a very promising tandem.

1. Introduction

Over the last two decades, the development of non-invasive *in vivo* imaging techniques has played a crucial role not only in clinical diagnosis, but also in preclinical research, both to assess the mechanism of disease development and to study the effects of medicines. In general, an imaging technique is expected to have not only high spatial resolution, but also a great depth of penetration. If we also want to gather molecular information, at cellular or sub-cellular level (molecular imaging), the techniques must be sensitive enough to detect targets present at very low concentrations, and therefore have excellent sensitivity [1]. The imaging techniques used in preclinical and clinical trials are Computed Tomography (CT), UltraSonography (US), Magnetic Resonance Imaging (MRI), nuclear imaging, in particular Positron Emission Tomography (PET) and Single-Photon Emission Computed Tomography (SPECT), and Optical Imaging (OI). CT, MRI,[1] and US, which are anatomical imaging methods, provide information about the anatomy of organs. SPECT, PET, and OI belong to the category of functional imaging techniques which are used to obtain molecular or metabolic information within a given tissue or organ [2a]. More recently, a new technology, photoacoustic imaging (PAI), based on optical excitation and ultrasonic detection has emerged in the arsenal of techniques, with high expectations in terms of contrast, resolution and depth of penetration [2b]. Consequently, we will go on to identify the salient features of the technique that make it so effective, and we will describe the most common contrastophores used in this imaging mode.

No single imaging modality can meet the triple objective of resolution, sensitivity and depth of penetration [3]. Only a combination of these techniques, building on their respective strengths, can meet this challenge. To avoid any biodistribution problems, it is also necessary to combine these different modalities within a single object [4]. Under these conditions, it should be possible to diagnose a given patient with all the relevant anatomical and functional information.

In this publication, we will begin with an overview of the different conventional imaging modalities describing the physical principles inherent in each technique. Based on these principles, we will establish a

* Corresponding authors.
** Corresponding author at: General, Organic and Biomedical Chemistry Unit, NMR and Molecular Imaging Laboratory, University of Mons, UMONS, B-7000 Mons, Belgium.
E-mail addresses: cyril.cadiou@univ-reims.fr (C. Cadiou), sophie.laurent@umons.ac.be (S. Laurent), francoise.chuburu@univ-reims.fr (F. Chuburu).

[1] MRI can also be used for functional imaging, but only the anatomical aspect will be discussed here.

https://doi.org/10.1016/j.ccr.2025.216523
Received 7 November 2024; Received in revised form 23 January 2025; Accepted 4 February 2025

set of specifications to be met by contrast agents (CAs) developed for each modality, and present recent examples of (*i*) molecular (*ii*) coordination complex-based and (*iii*) nanoparticle-based contrastophores. Finally, a few examples of multimodal probes whether molecular or nanoparticle in nature, based on improved performance in terms of resolution, sensitivity, and penetration depth, using for this purpose the MRI-PAI combination will be described. Readers will not be surprised to find no mention about targeted probes, nor environmentally sensitive probes (pH, temperature, ions, sensitive redox probes, *etc.*) or theranostic devices, as the aim here is to establish a link between the physical principles of the techniques and the improvement ways for signal enhancement that are currently being explored.

2. Conventional imaging modalities

2.1. Anatomical imaging techniques

2.1.1. Computed Tomography (CT)

Obtaining anatomical images after irradiating a subject with X-rays has its origins in W. C. Roentgen's seminal experiment in 1895, in the Physical Institute of the University of Wurzburg. It earned its discoverer the first Nobel Prize in Physics in 1901. The identification of this unknown radiation, named X for the occasion or *Röntgenstrahlung*, was an unexpected observation. When placed close to a Crookes discharge tube covered by a light-tight black cardboard envelope, Roentgen succeeded in making a platinum-barium cyanide screen fluorescent. Moreover, by placing various objects, including metal ones, between the tube and a photographic plate, he managed to obtain a snapshot of the objects, illustrating the fact that X-rays can penetrate matter. At Roentgen's first lecture to the Würzburg Physico-medical Society in 1896, he showed an X-ray of the conference chairman's hand. The transposition of physical experience to medical imaging was then launched [5]. Although conventional radiography has made a major contribution to medical diagnosis, its limitations led to the development of computed tomography (CT) in the early 1970s.

CT imaging is a 3-dimensional version of conventional X-ray radiography where the signals are processed to generate cross-sectional images. During a CT scan examination, ionizing radiations, X-rays, are delivered all around the body to generate an image based on hard tissue-induced attenuation. The X-ray beam is absorbed by the tissues according to their respective mass energy absorption coefficient (μ_{en}/ρ) which depends on their density and their molecular composition. Consequently, structures like bones, constituted of atoms of higher atomic numbers and then higher electron densities absorb more the incident radiation and exhibit opacification [6].

CT images are characterized by a very good resolution ($\leq$20 μm) a good penetration depth (>500 mm) [1,7a] but low contrast. They are preferably used to locate skull fractures and traumatic brain injuries [8] or to identify cancer locations [9]. Most of the body's soft tissues have the same capacity to attenuate incident X-rays, which means that the contrast between these tissues is poor. To improve this contrast, it is necessary to use contrast agents whose role is to reinforce these opacification capacities where they accumulate. Thus, the contrast agents used in X-ray imaging contain atoms of high atomic number such as iodine (Z = 53). The most common small-molecule iodinated contrast agents which are used in medical applications are low molecular weight (<2000 Da), low osmolality nonionic contrast agents [7b], derivatives of 1,3,5-triiodobenzene (Fig. 1) such as Iohexol (Omnipaque®, $C_{19}H_{26}I_3N_3O_9$, low osmolality), Iopamidol (Isovue®, $C_{17}H_{22}I_3N_3O_8$, low osmolality), Iosimenol ($C_{31}H_{36}I_6N_6O_{14}$, isomolar to plasma), Iodixanol (Visipaque®, $C_{35}H_{44}I_6N_6O_{15}$, low osmolality), and Iotrolan (Isovist®, $C_{37}H_{48}I_6N_6O1_8$, low osmolality) [10].

With an atomic number close to that of iodine, barium (Ba: Z = 56) can also be used in CT contrast agents like barium sulfate [11].

To improve the performance of conventional X-ray contrast agents, a new generation of nanometric X-ray contrast agents has been developed. This type of structure has several advantages, as it increases the concentration of iodine per object, thereby enhancing opacification capacity. Their pharmacokinetic properties are also interesting since their residence time in the bloodstream is increased and their renal clearance improved [7,12]. Stealth liposomes containing iodinated contrast agents but also nanosuspensions, nanoemulsions, nanocapsules, polymeric nanoparticles (micelles constituted from amphiphilic polymers or dendrimers) and iodinated metal-organic frameworks have been developed [7,12]. Among new nano-sized systems, nanoparticles based on atoms with a higher atomic number than iodine, such as gold nanoparticles or gold nanorods (Au: Z = 79) [7,11–13], bismuth nanorods (Bi: Z = 83) [14] but also lanthanide nanoparticles (Gd: Z = 64, Er: Z = 68, Yb: Z = 70) [15] are interesting radiopaque nanoparticulate contrast media that possess favorable X-ray attenuating properties.

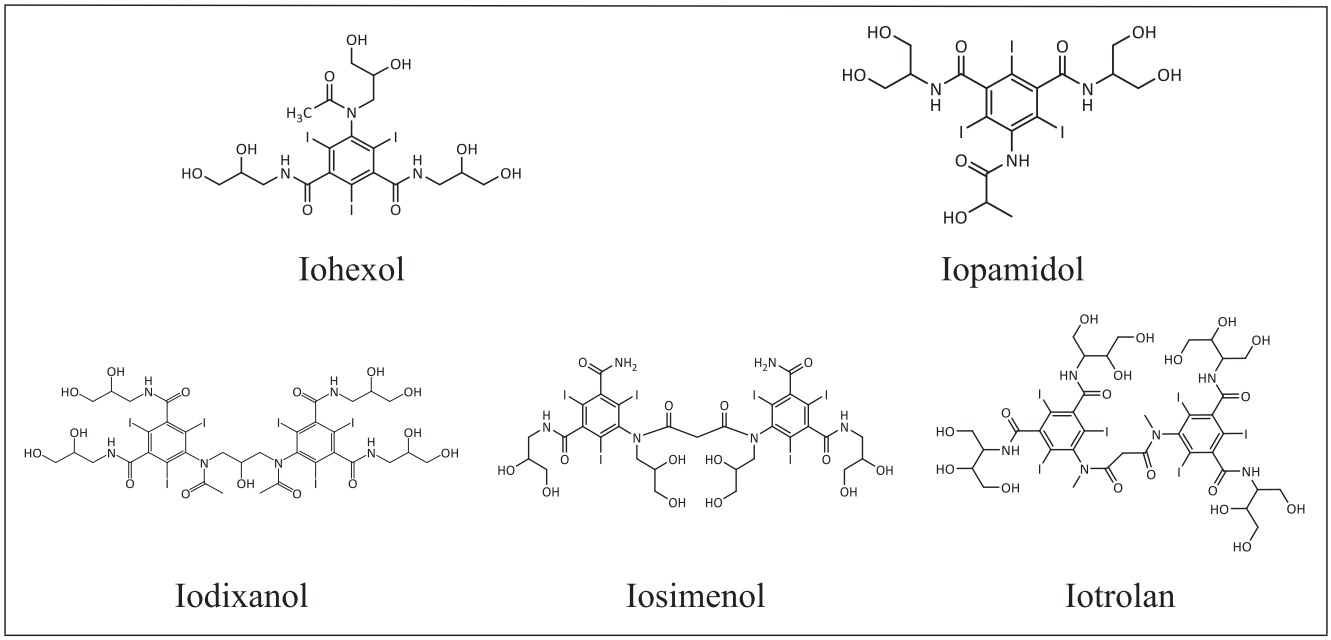

Fig. 1. Chemical structures of non-ionic iodinated CT contrast agents.

2.1.2. UltraSonography (US)

Ultrasound's history in medical applications [16] may begin with its use in undersea distance measurement and the experiments of J.-D. Colladon in Geneva. The 1820s saw, with the work of Lord Rayleigh, the development of methods for measuring the speed of sound in water and theories governing the physics of acoustic waves. The advent of the piezoelectric effect discovered by P. and J. Curie in the late 19th century marked a pivotal moment in the evolution of echo-sounding devices, facilitating the generation and reception of sound waves within the megahertz or ultrasound range. The two world wars that ensued subsequently precipitated the development of these systems for military purposes. The application of ultrasound in medical practice was initiated during and shortly after the Second World War. Beginning in the mid-1960s, the advent of commercial devices, facilitated by technological advances in electronics and piezoelectric materials, precipitated the rapid democratization of ultrasound imaging techniques [16b]. Even today, ultrasonography (or ultrasound imaging) is one of the most widely used medical imaging technologies and probably one of the less expensive.

This non-ionizing technique uses ultrasounds with frequencies between 20 kHz and 200 MHz. The US signal produced by a transducer, which can both emit, as well as detect the US echoes reflected (pulse-echo method) [17]. The principle of the technique is based on the reflection of the sound waves emitted by the ultrasonic transducer by the tissues, the intensity of this reflection being correlated to the acoustic impedances of the tissues (in other words their mechanical resistance to US waves). Interfaces between tissues of similar acoustic impedances usually generate low-intensity echoes (small acoustic impedance gradient). Conversely interfaces between biological tissues with very different acoustic impedances generate powerful echoes (large acoustic impedance gradient). If the acoustic impedance gradient between tissues is low, the intensity of the echo reflected by their interface will be low. In contrast, if this gradient is high, the reflected echo will be intense [17].

The advantage of US imaging is that soft tissues (such as nerves, muscles, tendons and vessels) can be visualized in real time. Its tissue penetration depth (several cms) can be tuned by the user, modifying the frequency, cycle, and exposure time. This can be an advantage but also a drawback since the result will be operator dependent. Moreover, this technique offers a poor resolution (~100–800 μm) [1,7], and as for the other imaging modalities, this aspect can be improved using contrast agents. US contrast agents are characterized by a large acoustic scattering cross-section, so that they scatter US waves more strongly than the surrounding blood or tissues. In the first experiments using intra-arterial injection of Ultrasound Contrast Agent (UCA), US signal improvement was attributed to the formation of small bubbles during the product injection [18]. This has fostered the development of bubble-based UCAs and particularly microbubbles (MBs). Microbubbles are gas-filled structures that make excellent reflectors because of their density and, above all, their compressibility. As MBs strongly reflect sound waves, they increase the quantity of these waves returning to the transducer and therefore increase the signal-to-noise ratio. The two main factors governing their interaction with US are the physical properties of the MB population *i.e.,* nature of the gas, rigidity of the capsule, mean diameter and distribution of the bubble population, and obviously the amount of acoustic power locally delivered [19]. Surface tension and preventing the dissolution of the gas core of MBs are the key points to master when designing microbubbles [20]. To this end, several solutions have been developed to stabilize MBs including the development of MB shells based on albumin, PLGA-type polymers or phospholipids. Currently, several MB-based US contrast agents are at various stages of development for intravenous administration, such as Echovist ®, Levovist®, Sonavist® [20]. However, the stability and the circulation time of these microbubbles are limited because of the high solubility of air in water. These issues have been addressed by replacing air with perfluorinated gases or sulphur hexafluoride (notably in Definity®, Optison®, Sonovue® and Sonazoid® products), which have limited solubility and diffusibility in water [20]. Further improvements have also involved producing microbubble suspensions that are better controlled in terms of dispersity (monodisperse microbubbles) [21] and targeting for molecular imaging [22].

However, due to their micrometric size, their short circulation time in blood vessels and low extravasation, these MBs can only produce contrast-enhanced US imaging inside the vascular system. To overcome these limitations, the most recent UCAs are nanometric in size [23] even though acoustic diffusion diminishes as the size of the bubble decreases. However, the stability of small bubbles, due to faster gas loss than that of larger bubbles, can pose problems [22d]. To overcome this, nanobubbles for which the shell was stabilized with surfactant [24], with block copolymer [20c,25], or lipids (bubble-liposomes) [20c,26] were developed.

2.1.3. Magnetic Resonance Imaging (MRI)

The development of magnetic resonance imaging (MRI) exemplifies the ongoing success of applying physicochemical techniques to medical contexts. This development of nuclear magnetic resonance (NMR), was first explored and quantified by the pioneering research of I. I. Rabi (Nobel Prize in Physics in 1944), followed by E. M. Purcell and F. Bloch developments (Nobel Prize in Physics in 1952) [27]. They have respectively developed a resonance method for recording the magnetic properties of atomic nuclei and demonstrated the NMR phenomenon in fluids and solids. A few years later, while working on diffusion studies in solids, E. L. Hahn developed spin echo techniques [27b], a pivotal tool for signal generation in magnetic resonance imaging (MRI). The first biomedical application of MRI was proposed by R. V. Damadian in 1970 who demonstrated that it was possible to distinguish tumors from normal rat tissues [27c]. Inspired by Damadian's work, P. Lauterbur showed that it was possible to obtain a two-dimensional cross-sectional image of a living mouse by encoding the spatial information of NMR signals with magnetic field gradients. Moreover, the echo-planar imaging technique and the mathematical processing and computing analysis of signals developed by P. Mansfield allowed to considerably reduce the acquisition times and make a few years later MRI usable at a clinical level. For these fundamental advances, Lauterbur and Mansfield were awarded the Nobel Prize in Physiology and Medicine in 2003 [27a].

Magnetic resonance imaging (MRI) is therefore one of the most widely used medical imaging modalities for non-invasive, atraumatic and reliable diagnosis. This non-radiative technique, characterized by an absence of limit in penetration depth [1,7], can produce high-resolution anatomical images (25–100 μm spatial resolution) which is of the uppermost importance for the early detection and localization of lesions [28]. Due to their nuclear spin, protons in tissue water molecules possess a magnetic moment and behave like small magnets. In the absence of a magnetic field B_0, these tissue protons, are randomly oriented to one another, and the resulting tissue magnetization is zero. In the presence of a magnetic field B_0, oriented in z, the protons will orient themselves relative to the field, while imparting a conical rotational motion - or precession - around it. The global population of nuclear spins will then split into two sub-populations, the majority of which will correspond to magnetic moments oriented parallel to B_0, and the minority will correspond to magnetic moments oriented anti-parallel to B_0. This difference in distribution results in a global tissue magnetization Mz, oriented in the same direction as the B_0 field. If a radio-frequency pulse is applied to the precessing spins, and if the frequency of the pulse is equal to the precession frequency of the spins around B_0, then the pulse's energy will be transferred to the spins. As a result, the tissue magnetization M_z will shift in the transverse plane *xy*, perpendicular to the axis of orientation of B_0. If the radiofrequency stimulus is released, the tissue magnetization M_z will return to its equilibrium position along z, in the direction of B_0 [29]. This return to equilibrium, which corresponds to the relaxation phenomenon, will be characterized by relaxation times, one being the longitudinal relaxation time T_1, which represents the time required for the tissue magnetization M_z to recover

its initial position along the z axis, and the other, the transverse relaxation time T_2, which corresponds to the time required for the magnetization in the *xy* plane to collapse. The T_1 and T_2 relaxation times of tissue protons are tissue-dependent. For instance, for an external field of 3 T, average T_1 relaxation times of grey and white matter are 1331×10^{-3} s and 832×10^{-3} s respectively while average T_2 relaxation times of grey and white matter are 80×10^{-3} s and 110×10^{-3} s respectively [30]. MRI allows to visualize these differences, both in T_1 and T_2, and the resulting contrast between different soft tissues is superior in comparison to CT or US imaging modalities. However, even if these two relaxation mechanisms are used in MRI through T_1-weighting and T_2-weighting sequences, T_1 images are characterized by a better signal-to-noise ratio which is why they are so interesting.

Healthy and pathological tissues are sometimes difficult to distinguish, and contrast enhancement is necessary in many cases (including detecting tumors, inflammation, and infection). The solution consists then in increasing selectively the signal returned by the pathological tissue, by the administration of CAs. Two types of contrast agents are available: T_1 contrast agents and T_2 agents. The role of T_1 contrast agents is to decrease the longitudinal relaxation time (and thus accelerate the relaxation speed) of protons in tissue water molecules. The result is an increase in contrast through image brightening. T_2 contrast agents decrease the transverse relaxation time and have the opposite effect (image darkening). T_1 relaxation is greatly decreased in the presence of paramagnetic substances, *i.e.,* those carrying unpaired electrons such as Gd(III) ion ([Xe]$4f^7$ electronic configuration *i.e.* seven unpaired electrons and symmetrical electronic ground state) [31], while the most common T_2-contrast agents are superparamagnetic iron oxide nanoparticles (SPION) [32]. To date, the commercially available MRI contrast agents are discrete Gd chelates (also known as Gadolinium-Based Contrast Agents, GBCAs). Indeed, since Gd(III) ion is significantly toxic in its aqua-ion form [31], its clinical use depends on its chelation within linear or macrocyclic polyaminocarboxylate ligands (Fig. 2) [33]. The parameter used to assess how effectively GBCAs brighten images is relaxivity r_1. It corresponds to the reduction of the water proton's relaxation times (T_1) brought about by a 1 mM concentration of Gd ions. Thanks to their ability to enhance the contrast of MRI images, these complexes are also used for direct image guidance during radiotherapy treatment to ensure better anatomical alignment of the patient and facilitate daily adaptation of the treatment plan [34].[2]

However, it should be noted that the European Medicines Agency has recently withdrawn from the market or restricted the use of linear chelate-based contrast agents [33b]. Their *in vivo* stability has been called into question. Indeed, their ability to trap gadolinium permanently has been compromised and gadolinium depositions in different organs (*e.g.*, brain, skin, liver, and bone) due to its demetallation have been demonstrated [35]. For these reasons, research in the field of paramagnetic contrast agents has focused on the development of gadolinium chelates that exhibit a higher relaxivity, which should enhance their efficacy and reduce the doses injected [36]. Alternatives to the gadolinium ion have also been explored, and high spin Mn(II) (5 unpaired electrons [37],) or high spin Fe(III) (5 unpaired electrons [37g,38],) chelates are being developed for T_1 MRI. Paramagnetic inorganic nanoparticles or nanoparticles incorporating paramagnetic complexes are also part of these alternatives and several recent reviews provide a good overview of these nanosystems [39]. Among paramagnetic inorganic nanoparticles, gadolinium oxide (Gd_2O_3), gadolinium fluoride (GdF_3), gadolinium phosphate ($GdPO_4$), and manganese oxide (MnO) nanoparticles have been investigated as T_1 contrast agents [39a–i]. To enhance their colloidal stability and to improve their biocompatibility these systems are most of the time coated with mesoporous silica and functionalized with PEG chains of different lengths. Ultra and extremely small iron oxide nanoparticles (USPIOs and ESIONPs) also display a T_1-type behavior. [39h] An alternative to metal nanoparticles is to combine paramagnetic chelates, mainly Gd(III) chelates, with nanoparticles to increase the chelate relaxivity [39j–l]. Several strategies have been developed in this respect, including grafting, anchoring paramagnetic chelates to the surface of nanoparticles, or embedding these chelates within nanoparticles. Various nanomaterials have been used in this context such as modified natural nanoparticles, self-organized aromatic polyaromatic peptides, lipidic self-assembled nanostructures, dendrimers, mesoporous silica, and polymeric nanoparticles [39j–m]. For all these systems the increase in relaxivity by Gd chelate results in a much lower concentration of Gd required to achieve contrast. It should also be pointed out that the most effective strategy is to immobilize the chelates' global and local rotational movements by burying them in water-porous matrices. In this context, hydrogels, widely used to develop devices that interact intimately with biological organisms [40] constitute interesting systems. Indeed, hydrogels are characterized by a 3D polymer network formed through physical or chemical crosslinking surrounded by an aqueous solution. This structure confers to hydrogels good viscoelastic properties and their high-water content gives them attributes like those of liquids. These characteristics are perfectly in line with the specifications established to improve the relaxivity of GBCAs. As a result, nanohydrogels encapsulating Gd chelates have recently been developed as hypersensitive MRI probes [41]. When these paramagnetic complexes are embedded in a hydrogel matrix constituted of chitosan (CS) and hyaluronic acid (HA), a huge enhancement of the r_1 relaxivity per Gd ion is obtained between 10 and 60 MHz (r_1 (20 MHz) = 22.0, 28.6, 62.4, and 78 mM^{-1} s^{-1} for GdDTPA, GdDOTA, GdAAZTA and GdDOTP nanosuspensions respectively). In these nanohydrogels structures, the entrapment of Gd chelate results in a reduction of the rotational tumbling motion of the chelate, mediated by the viscosity of the aqueous solution within the hydrogel matrix [41a–i]. Thermodynamic and NMR measurements have highlighted that the interaction between the polymer matrix, metal chelates, and water induces a reorganization in the mesh-like structure of the hydrogels and the formation of nano-compartments in which water is in an unusual aggregate state. Moreover, multiple Gd chelate-water interactions are developed between the exchangeable protons of the water molecules coordinated to the Gd chelate and the other water molecules trapped within the hydrogel structure (freely moving water molecules or water molecules bonded to the polymer chains). A careful analysis of the relaxation data for Gd chelates encapsulated within nanohydrogels emphasizes the fast diffusion of the water molecules into the hydrogel structure and demonstrates that the exchange of water molecules with the surrounding water is fast enough not to hinder relaxivity [41e,f]. A similar analysis can be performed for nanogels incorporating Mn chelates [41g]. Consequently, embedding GBCAs within the chitosan-hyaluronic acid hydrogel matrix results in a significant amplification of the magnetic properties of Gd chelates (hydrodenticity concept) [41h, i], which appears to be promising for the development of nanoprobes with excellent MRI signal enhancement performance [42].

2.2. Functional imaging techniques

2.2.1. Single Photon Emission Computed Tomography (SPECT) and Positron Emission Tomography (PET)

These two imaging modalities used in nuclear medicine detect the radiation emitted by radioactive substances (or radiotracers) injected into the body. Although the use of radiotracers had already been implemented, particularly since the work of G. de Hevesy (Nobel Prize in Chemistry in 1943) [43], the beginnings of SPECT and PET date back to the 1960s with the pioneering work of D. E. Kuhl, S. Rankowitz and co-workers [43b]. Significant improvements were achieved in the following years, attributable to the contributions of A. M. Cormak and G. N. Hounsfield, who developed high-performance image reconstruction algorithms [43b]. Subsequently, an enhancement in sensitivity was achieved through the modification of the detection systems, including

[2] Complex charges and coordinated water molecules are omitted for clarity.

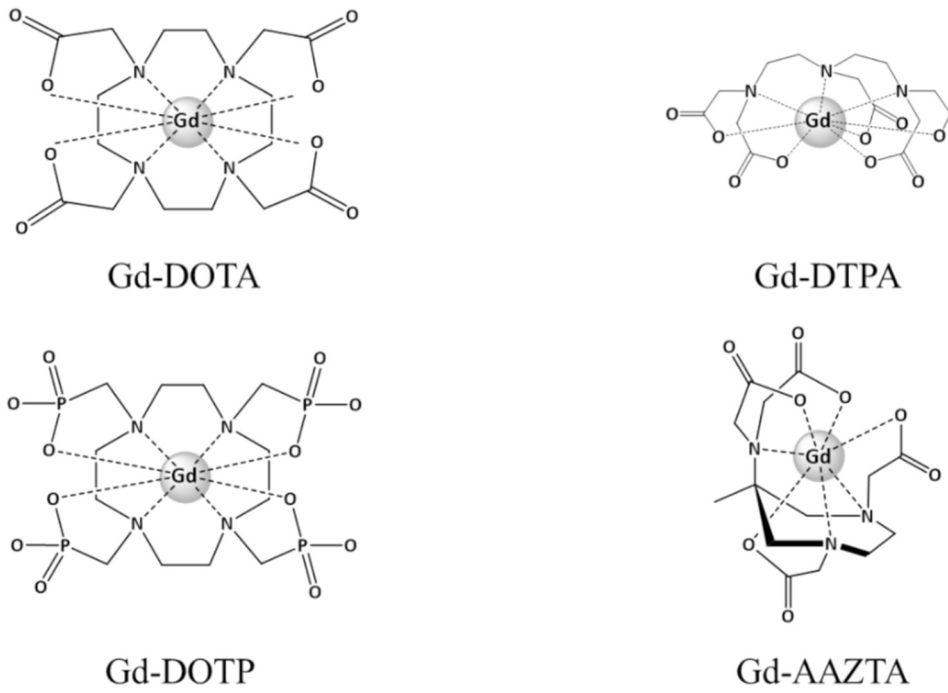

Fig. 2. Chemical structures of some representative linear and macrocyclic Gd chelates (GBCAs).

the multiplication of detectors in SPECT and the modification of detection system geometry in PET [43]. The images thus obtained give information based on the spatial concentration of injected radiopharmaceuticals and provide quantitative (picomolar-scale) biological evaluation of regional tissue function *in vivo*. Clinical applications of PET and SPECT are found in oncology, cardiology, neurology, and psychiatry. However, the spatial resolution of emission tomography is relatively poor compared to other modalities such as CT or MR.

Radionuclides used in SPECT imaging are single-photon emitters (γ rays), that are detected by a gamma (γ) camera. To obtain an image of a volume, the γ camera rotates around the body and collects a set of overlapping two-dimensional images, to build up the final three-dimensional image. For SPECT-based imaging, the radionuclide should emit one γ-ray per decay (100 % γ-emission yield) with energies between 100 and 370 keV (to prevent cellular damages, while still being energetic enough to penetrate the body completely), and with a convenient half-life (between 6 h and 3 days). The most common SPECT radionuclides are technetium-99 m (^{99m}Tc, half-life $t_{1/2}$ = 6 h, γ-ray emission energy 141 keV), ^{123}I ($t_{1/2}$ = 13.2 h, γ-ray emission energy 159 keV), ^{67}Ga ($t_{1/2}$ = 78.2 h, γ-ray emission energy 93 keV), ^{111}In ($t_{1/2}$ = 67.2 h, γ-ray emission energy 171 keV), and ^{201}Tl ($t_{1/2}$ = 73 h, γ-ray emission energy 167 keV) [44]. Among these radioelements, ^{99m}Tc has a special status since its decay is long enough to handle the radiolabeling and imaging process and short enough to protect patients from exposure to unnecessary radioactive doses once the examination has been completed [44]. Lastly, its practical production method, using a transportable ^{99}Mo/^{99m}Tc generator, makes it easy and inexpensive to supply [45].

Radionuclides used in PET imaging are positron (β^+ particle) emitters. Positron decay occurs with neutron-poor radionuclides and consists of the conversion of a proton into a neutron with the simultaneous emission of a positron (β^+) and a neutrino (ν). The short-lived positron undergoes an annihilation reaction with a neighboring electron, producing two high-energy photons (E = 511 keV) emitted approximately 180° apart. PET detection then relies on the detection in coincidence of these γ-photons by an array ring of detectors, each detector being paired with another located 180° away from it. By comparison with SPECT, the use of this coincidence detection method considerably improves sensitivity while ensuring excellent tissue penetration.

The most common PET radionuclides are short-lived β^+ emitters such as ^{11}C ($t_{1/2}$ = 20.4 min), ^{13}N ($t_{1/2}$ = 10 min), ^{15}O ($t_{1/2}$ = 2 min), and ^{18}F ($t_{1/2}$ = 110 min). ^{11}C, ^{13}N, and ^{15}O are mostly used for labeling organic small molecules since these atoms are core elements in biology. In the same way, ^{18}F can substitute a hydrogen atom by a bioisosteric replacement and fluorodeoxyglucose (^{18}FDG) is the prototype of the ^{18}F-labelled compounds family. Detailed radiochemical methods used to synthesize small molecules bearing ^{11}C, ^{13}N, ^{15}O are provided in recent reviews [46]. Metal radionuclides (or radiometals) such as ^{64}Cu ($t_{1/2}$ = 12.8 h), ^{68}Ga ($t_{1/2}$ = 67.6 min), ^{89}Zr ($t_{1/2}$ = 78.4 h) and ^{111}In ($t_{1/2}$ = 67.2 h) are rather used for labeling biomolecules such as peptides, or antibodies to target cells with high selectivity and affinity. In these cases, metal radionuclides need to be chelated [46d,47].

'Free' radiometals, whether they are intended for SPECT or PET imaging, need to be sequestered by organic ligands to prevent their toxicity. The safest way to use these radiometals *in vivo* is to complex them with bifunctional chelating agents (BFCAs) [48]. BFCAs are molecules consisting of two distinct parts, one dedicated to chelating the metal as strongly as possible, and the other, a carrier molecule, that can be covalently coupled to targeting molecules of interest. This assembly is defined as a radiopharmaceutical. It should also be noted that, depending on the nature of the chelating group, this bifunctional architecture can also be used to complex lanthanides for MRI or optical imaging purposes. Linkers, useful for modifying the pharmacokinetic profile of the radiopharmaceuticals but also used to distance the chelating part to the carrier molecule are used as bridges (Fig. 3). The nature of the chelating unit depends on the radiometal chemical demands (ligand donor atom preferences according to Pearson's hard and soft acids and bases theory, coordination number, and coordination geometry) [48]. A significant number of BFCAs have been developed to meet the constraints of efficient radiometal coordination and some recent developments can be found in the references [49]. Among the prospective chelators, macrocycles bearing extra coordinating pendant arms such as DOTA, TETA, NOTA, PCTA, MACROPA, and their derivatives [49a–d,g–j] have enabled a good control of radiometal coordination.

Nanomaterial-based formulations can also provide high-

	$t_{1/2}$	$E_{\gamma\ rays}$ (eV)
^{99m}Tc	6 h	141
^{123}I	13.2 h	159
^{67}Ga	78.2 h	93
^{111}In	67.2 h	171
^{201}Tl	73 h	167

	$t_{1/2}$		$t_{1/2}$
^{11}C	20.4 min	^{64}Cu	12.8 h
^{13}N	10 min	^{68}Ga	67.6 min
^{15}O	2 min	^{89}Zr	78.4 h
^{18}F	110 min	^{111}In	67.2 h

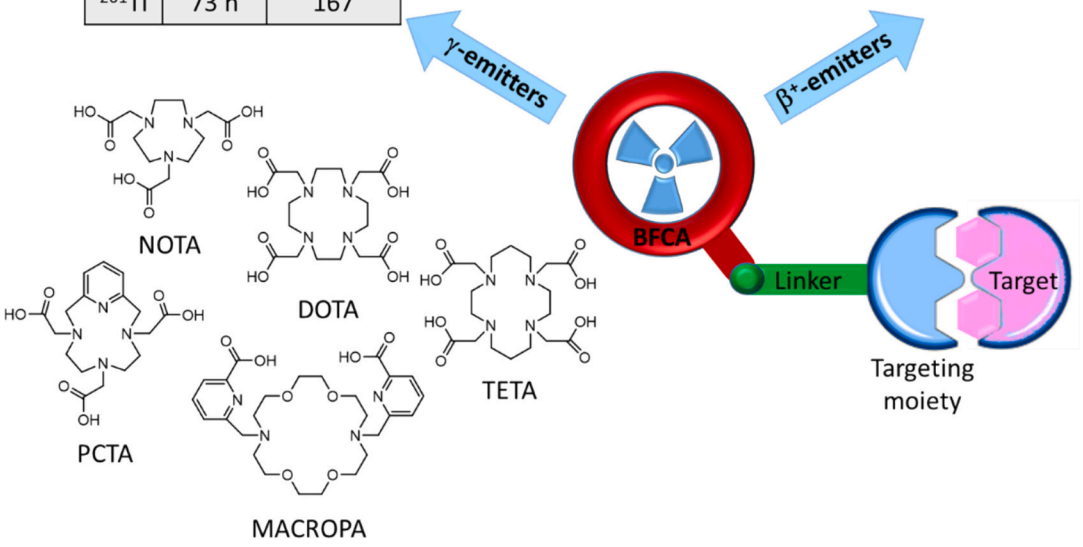

Fig. 3. Bifunctional chelating agents (BFCA). a- Selected radionuclides for SPECT and PET imaging (in the Tables). b- Chelators for inorganic labeling bifunctional chelating agents (structures bottom left).

performance solutions for use in SPECT and PET imaging. Organic (liposomes, protein-based, polymeric micelles, dendrimers, and polymers) or inorganic nanomaterials (C-based nanomaterials, metal-based nanomaterials, Si-based nanomaterials) have been developed with this in mind [50]. A special feature of radiometal labeling of nanomaterials, is that the time required to synthesize and purify nanomaterials must be compatible with the lifetime of the radiometals used. Various strategies that can be divided into three categories, *i.e.,* (*i*) nanomaterial surface labeling, (*ii*) incorporation of radioelements into nanoparticles or (*iii*) at the interface between nanomaterials and ligands, have been implemented to this end. Those three strategies are described in detail in the references [51].

2.2.2. *Optical Imaging (OI)*

Optical imaging is another non-invasive diagnostic method based on the detection of photons emitted by luminophores administered to patients. While the development of dedicated microscopes dates back to the early 20th century, the phenomenon of light emission excited the curiosity of scientists in the 1800s. Blue light emission from a colorless quinine solution when illuminated by the sunlight under certain incidence had already been demonstrated almost simultaneously by Sir J. Herschel and Sir D. Brewster in the mid-1800s [52a,b]. The luminescence of calcium fluoride already well-documented, and that of calcium sulfite was also observed by E. Becquerel [52c], who in 1842 established that emitted light has a longer wavelength than incident light. In 1852, Sir G. G. Stokes formalized the phenomenon (Stockes' law), and coined the term "fluorescence" to describe it [52c].

Photoluminescence (including fluorescence and phosphorescence) is one of the most used optical modalities because of its high sensitivity, its good specificity, and its low limit of detection. The distinction between fluorescence and phosphorescence, as proposed by F. Perrin in 1929, was later formalized in the renowned Jablonski diagram (1935, [52a]). Fluorescence relies first on the absorption of a photon by a given luminophore. This luminophore will absorb light if the energy of the incident photon matches with the energy difference between the singlet electronic ground state of the luminophore (S_0) and an excited electronic state of higher energy. After a brief delay of time, the excited-state luminophore undergo relaxation to the ground state *via* various photoemissive mechanisms. For fluorescence emission, the relaxation takes place an excited singlet state S_1 to the ground state S_0, and during this process the spin multiplicity is preserved. Phosphorescence is another emission mechanism which involves relaxation between an excited triplet state T to the ground state S_0 and, in this case, there is a multiplicity change during relaxation [53].

Optical imaging uses photons with wavelengths ranging from the visible to the near infrared (NIR) (500 to 1500 nm wavelength) [54]. The optical signal within the visible range (400–700 m) is limited to imaging the surface and its proximity (*i.e.*1–2 mm depth), due to the absorption of light by oxy- and deoxy-hemoglobin (HbO_2 and Hb exhibit large absorption bands between 500 and 600 nm, see Fig. 6 below), water, and tissue constituents. For *in vivo* imaging, wavelengths in the NIR windows are preferable because in these ranges light scattering and absorption by tissue constituents are minimized. The first NIR window (NIR—I, 650–900 nm) offers good characteristics, as tissues have minimal absorption and minimal background autofluorescence, and provides the best visualization of deeper structures (up to 2 cm from the surface) [54]. However in this region, scattering remains important. The second NIR window (NIR-II, 1000–1800 nm), often split into the NIR-IIa (1000–1350 nm range) and NIR-IIb (1500–1800 nm) allows the *in vivo* luminescence contrast improvement. Indeed, in this wavelength range, light absorption and scattering are greatly reduced (compared to NIR—I), while autofluorescence is also reduced. Consequently, resolution and in-depth imaging are improved, enabling the observation of deeper tissues with higher spatial resolution. Finally, despite NIR-IIb light absorption by water is slightly stronger than in the NIR-I region, photon scattering and autofluorescence are even less important, enabling unprecedented improvements in detection depth, resolution, and sensitivity [55].

Because most tissues generate no NIR fluorescence contrast, NIR-fluorescence imaging usually requires the use of NIR-fluorescent probes (or NIR-fluorophores) [56]. Their absorption and luminescent wavelengths must match the regions where tissues feature minimum absorption and autofluorescence, *i.e.*, as mentioned above, in the NIR-I and NIR-II regions. The most studied exogenous NIR probes are small fluorescent molecules (Fig. 4), and among them cyanines (conjugated polymethine framework with an odd number of carbon atoms terminally disubstituted by nitrogen-containing heterocycles) [56c–e], rhodamine derivatives (whose xanthene core is modified to shift the emission wavelength to NIR) [51c–e,f], BODIPY-based probes (whose 3 and/or 5-positions are substituted by a styryl substituent for instance) [56c–e], squaraine-based probes [56c–e], croconaine dyes (based on donor-acceptor-donor structure), [56g] porphyrin and phtalocyanine derivatives [56c–e] However to date only two fluorophores are clinically approved, methylene blue (MB; λ_{abs} = 664 nm, λ_{em} ~ 680 nm), and indocyanine green (ICG; λ_{abs} = 785 nm, λ_{em} = 810 nm) [57].

Fluorescent metal complexes [58] and particularly lanthanide metal complexes [59] are another important class of probes with unique luminescent properties, including metal-centered emission, long luminescence lifetime that allows discrimination of the lanthanide complex signal from autofluorescence, large Stokes shift (*i.e.*, shift between the emission wavelength and the absorption wavelength), and high resistance to photobleaching. Trivalent lanthanide ions have a [Xe]$4f^n$ electronic configuration and their luminescent properties originate from 4f-4f transitions, $4f^n \rightarrow 4f^n5d^1$ transitions, and charge transfer transitions between the metal and its chelate (MLCT or LMCT). The main requirement to generate a sufficient lanthanide emission is to sensitize them with an appropriate organic chromophore, which has the role to absorb excitation light and to transfer the resulting energy to the accepting levels of luminescent lanthanide cations ("antenna effect"). The energies of lanthanide electronic levels differ from one lanthanide to another, leading to sharp emission bands associated to 4f-4f metal-centered transitions. These wavelengths vary from the visible to NIR range according to the lanthanide. For a given lanthanide they have a constant value, which is very useful for imaging because their position is insensitive to the chemical or biological environment [58,59].

Besides these small fluorescent probes, water-soluble fluorescent polymers constituted of π-conjugated backbones (*i.e.,* a delocalized electronic structure that exhibits efficient coupling between its segments), and terminal charged groups (which can be functionalized with a variety of recognition elements) have been developed for *in vitro* but also *in vivo* fluorescence imaging [60].

Recently, new luminescent concepts have emerged to improve NIR probes efficiency. One of the very first important development concerns the design of two-photon absorbing, NIR-emitting fluorescent probes [61]. This concept has gained in importance since the advent of NIR laser sources. Two-photon absorption and in general multiple photon absorption are a non-linear process involving the simultaneous absorption of two (or multiple) photons whose combined energy is sufficient to induce a molecular transition to an excited electronic state. For example, two-photon fluorescence occurs when two less energetic photons are simultaneously absorbed. Two-photon absorbers - NIR emitters (*i*) are generally made up of extended π-conjugated systems with, wherever possible, a fully planar architecture, and (*ii*) are also the site of intramolecular charge transfer *via* the grafting of donor groups (D) on one side and acceptor groups (A) on the other [61].

The second development concerns the aggregation-induced emission (AIE) concept and the design of AIE luminogens (AIEgens) [62a]. AIEgens exhibit weak or no fluorescence in solution but emit strong

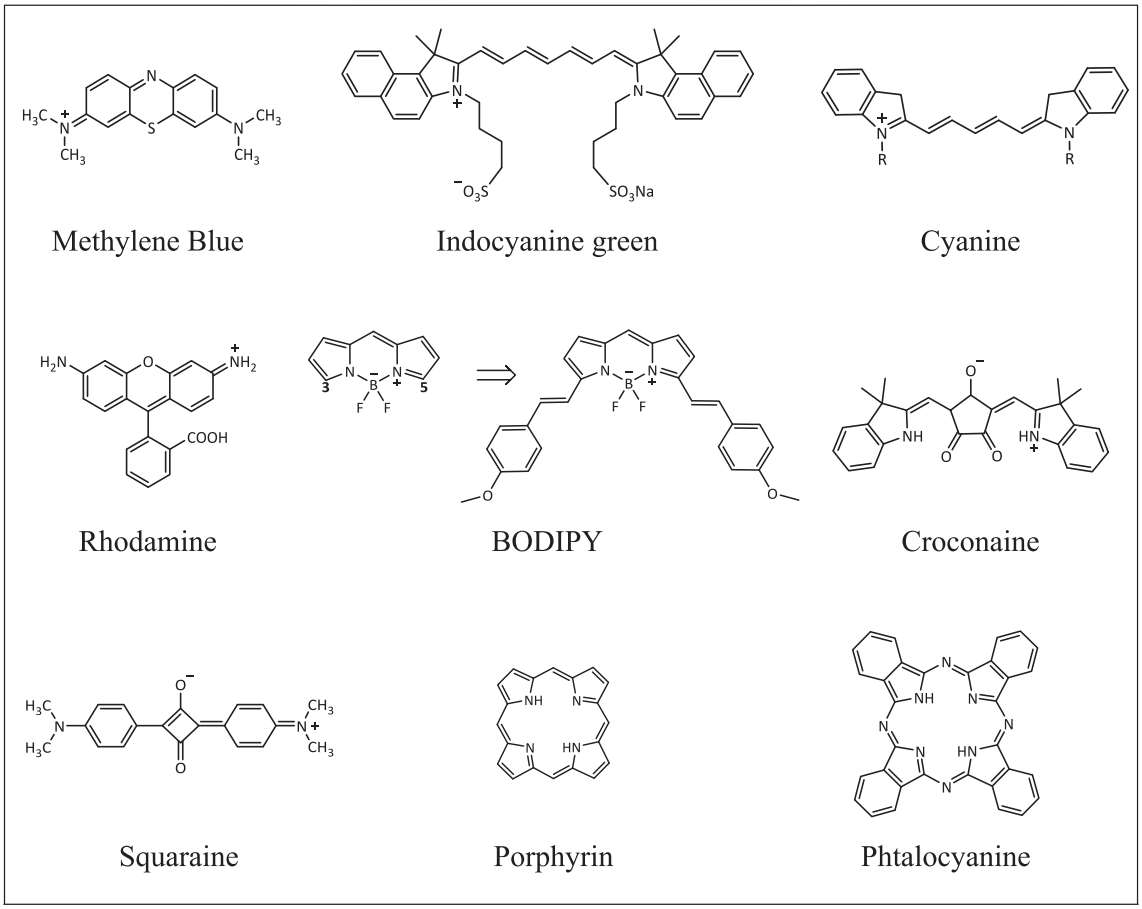

Fig. 4. Basic chemical structures of NIR probes.

fluorescence signals in the NIR range upon formation of sterically hindered aggregates [62]. AIEgens have a similar structure as NIR-2photons absorbers *i.e.,* a π-conjugated backbone with donor-acceptor (D-A) architecture. In the transition from the isolated to the aggregated state, the conjugated system carrying the intramolecular charge transfer system is prevented from intramolecular rotations and vibrations, which promotes radiative decay, and then emission in the NIR.

A third possible development is fluorescent nanomaterials [55,63]. They include quantum dots (QDs) [55b,64], organic semi-conducting materials (OSM) and AIEgens encapsulated in nanoparticles [65], single-wall carbon nanotubes (SWCNTs) and carbon dots (CDs) [55b,66], gold nanoparticles (AuNPs) [67], rare-earth based up-conversion nanoparticles (UCNPs) [68]. Most of these nanomaterials are constituted of heavy metals (Cd, Te, Pb for QD, Au for AuNPs) or C (for SWCNT and CD), and Ln^{3+} ions (for UCNPs), and the safety of several of them is still controversial. This means that more detailed toxicity studies are needed, and improvements in their biocompatibility are a prerequisite for their routine use *in vivo*.

3. PhotoAcoustic Imaging (PAI)

The history of photoacoustic imaging dates to 1880, when A. G. Bell discovered the photoacoustic (PA) effect. At that time, Bell was working with his assistant C. Tainter on another means of communication, the photophone, which was designed to produce acoustic waves by irradiating a photosensitive selenium crystal with light, and thus wirelessly transmitting voice messages. This result was generalized when it was demonstrated that the illumination of different solid substances, but also of absorbing gases, with a rapidly interrupted beam of light energy resulted in the emission of acoustic energy at the same frequency as the modulation frequency [69]. However, due to the limited power of the light sources available at that time and low energy conversion rates, the acoustic emissions obtained were too weak to be detected by the existing instruments. In the 1990s, the development of pulsed laser light sources and acoustic detection equipment led to considerable improvements in sensitivity, enabling photoacoustic imaging to enter the biomedical field. In the following paragraph a few physical elements for understanding the propagation of light energy in optically scattering media such as biological tissue will be introduced.

3.1. General principle

Photoacoustic imaging (PAI) combines optical excitation and ultrasound (US) detection. In PAI, a light beam (nanosecond pulsed laser - pulse duration <10 ns) is sent onto the surface of the tissue. The light beam's energy is then repeatedly absorbed and scattered by chromophores. From a mechanistic point of view, absorbed optical energy excites electrons in chromophores from ground states to excited states. Excited electrons return to their ground state, releasing energy either in radiative form (the same mechanism as described for fluorescence emission, see above) or as thermal energy. (Fig. 5) This second mechanism induces thermoelastic expansion of the surrounding tissue, leading to a local increase in pressure and the emission of acoustic waves. These two mechanisms are not decorrelated, which implies that for PAI, thermal conversion efficiency must be favored at the expense of fluorescence.

The advantage of outgoing acoustic waves is that they are much less attenuated and scattered by tissues than photons. As a result, the output acoustic signal recovered by the transducers is better than that of an optical signal [70].

3.2. Penetration depth and spatial resolution

In PAI, tissue penetration depth depends on the attenuation of incoming photons and outgoing acoustic waves. In most soft tissues, optical attenuation dominates and according to the incident wavelength, the chromophores (*e.g.*, hemoglobin) present in the body will absorb the light beam to a greater or lesser extent. Therefore, in the choice of wavelength range, it is important to favor wavelengths where light absorption by the tissues is at the minimum, *i.e.*, as with optical imaging, in the near-infrared range (NIR). For example, using an excitation wavelength of 800 nm and without the use of contrast agents, mammary vascularization was observed down to a depth of 4 cm [71]. The penetration depth can be increased if PAI contrast agents that strongly absorb in the NIR range are used [72].

PAI spatial resolution depends on the frequency components of the acoustic wave reaching the detector, and not on the signal generation process itself because of the nature of the laser pulses used (frequencies between 10 and 100 MHz). The main factor limiting spatial resolution will be the acoustic attenuation present in soft tissues, and this resolution will decrease with penetration depth [73].

3.3. Photoacoustic imaging modalities

PAI can be divided into several categories: photoacoustic tomography (PAT) which is the traditional mode of PAI, photoacoustic microscopy (PAM) and their associated techniques. These categories within PA imaging are differentiated at the instrumental level rather than at the level of fundamental methodology.

In PAT, a large-diameter pulsed laser beam is used to illuminate the tissue surface.

Acoustic waves are detected using detectors placed at different points around the target tissue. Different types of geometry are commonly used for detection [74–77]. Spherical geometry allows, at least in theory, perfect reconstruction of the initial pressure distribution since acoustic waves are detected in all directions in space. However, the installation of such detectors is not always straightforward and for this reason, many PA scanners use arc-shaped focused detector arrays [77].

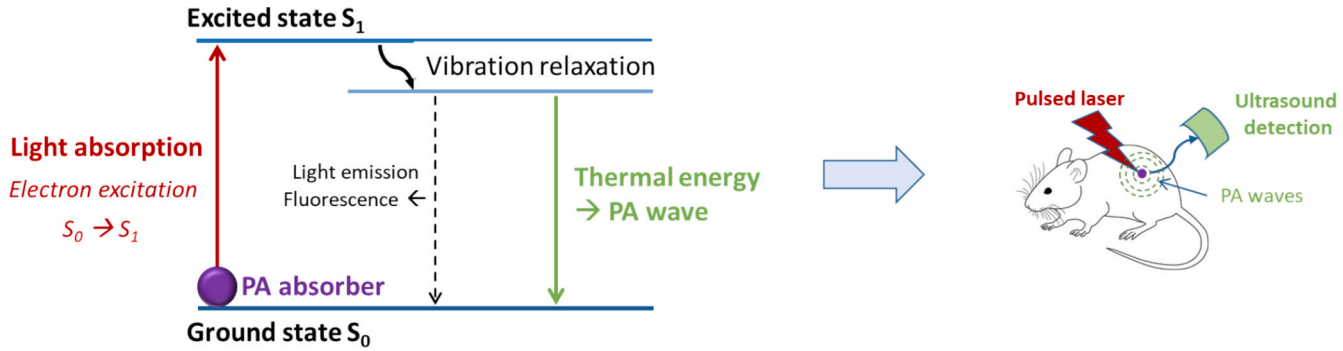

Fig. 5. Electron de-excitation pathways after absorption of an incident light showing the two competitive relaxation mechanisms *i.e.* fluorescence and heat release (inspired from Ref. [70]).

In PAM, the image is obtained by mechanically scanning the focused laser beam or the focused ultrasound detector. Unlike PAT, PAM does not require a reconstruction algorithm to obtain the PA image. PAM is divided into two sub-categories: optical-resolution photoacoustic microscopy (OR-PAM), and acoustic-resolution photoacoustic microscopy (AR-PAM) [78]. For OR-PAM, focusing will take place at the level of the excitation light beam, offering very high spatial resolution. Optical diffusion will limit the imaging depth to 1 mm, which is comparable to optical microscopy. For AR-PAM, a relatively large area is illuminated and focusing takes place at the level of the ultrasound detector. The imaging depth in biological tissue is greater than for OR-PAM (3 mm) [78].

If we are to compare the performances of PAM and PAT in terms of penetration depth and spatial resolution, PAM techniques offer a high spatial resolution (sub-micron spatial resolution) at the expense of penetration depth while PAT techniques offer the greatest depth of penetration into the tissues (cm) and a spatial resolution of a few hundred microns.

Multi-spectral optoacoustic tomography (MSOT) is one of the PAT techniques. It involves the illumination of the sample of interest with light pulses of different wavelengths and recording the ultrasound waves generated by the various photosensitive molecules [79]. This technique is then able to differentiate between different endogenous photoabsorbers and exogenous administered probes thanks to spectroscopic analysis. For that, exogenous optical agents must have spectral characteristics sufficiently distinct from those of the endogenous chromophores so that the signal can be extracted by spectral subtraction (at least in the first instance). Different exogenous optical agents have been used for this purpose and will be presented in the following section.

3.4. Contrast agents for photoacoustic imaging

3.4.1. Endogenous contrast agents

In the human body, it is possible to visualize the anatomical characteristics of tissues containing endogenous PAI chromophores such as hemoglobin, lipids, melanin, and water. Hemoglobin and melanin, which absorb much more than the other endogenous chromophores, are considered a primary source of contrast (Fig. 6).

As shown in Fig. 6, hemoglobin, and more specifically oxy- and deoxy-hemoglobin, dominates the absorption of the light beam for wavelengths below 1000 nm. Hemoglobin absorption is therefore used in PAI to visualize the vascular system [80]. Melanin has a higher absorption coefficient than hemoglobin but is localized in well-defined areas (skin, retina) and therefore in fewer tissues. For these reasons,

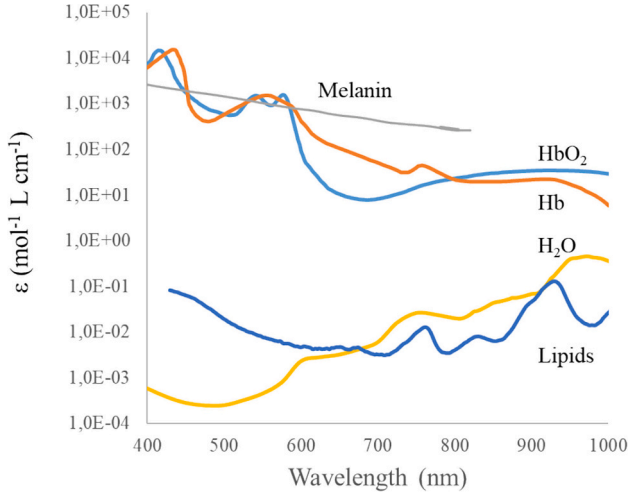

Fig. 6. Optical absorption spectra of endogenous chromophores in tissues. Adapted from http://omlc.ogi.edu

melanin does not dominate contrast in PAI as hemoglobin does, but it can be useful for visualizing the pigmented epithelium of the retina, and certain pigmented lesions in the skin [81]. However, it is possible to exploit chromophores that absorb less, such as water and lipids, thanks to their characteristic spectral signatures [82]. The absorption peaks for lipids are around 920, 1210, and 1710 nm. These absorptions allow to localize lipid deposits such as those found in atherosclerotic plaques [83].

In addition to endogenous chromophores, the injection of exogenous chromophores that absorb visible and near-infrared wavelengths can provide additional sources of contrast in PA imaging. Different examples will be described in the following section.

3.4.2. Exogenous contrast agents

For the contrast of exogenous agents to be maximal, it is important to minimize the contribution of endogenous contrast agents present in the tissues. The optical absorption of biological tissues is minimal in the NIR region ranging in the biological transparency window *i.e.*, from 700 to 1100 nm. Therefore, exogenous contrast agents must (i) absorb light in the NIR, (ii) have a high molar absorption coefficient in this frequency range and a high thermal conversion, while (iii) having a low fluorescence quantum yield, and (iv) be biocompatible. The family of PAI exogenous agents is subdivided into organic and inorganic agents [84].

Inorganic contrast agents: They include noble metal nanomaterials, carbon-based nanomaterials, and transition metal chalcogenides (TMC). Illumination of metallic nanomaterials enables high absorption of optical signals as well as a strong conversion of light into heat thanks to the phenomenon of localized surface plasmon resonance (LSPR). This phenomenon takes place when the frequency of the incident photons corresponds to the frequency of electron oscillations in the conduction band of metals, generating a strong optical absorption. Among metallic nanomaterials, gold-based nanomaterials exhibit very good plasmonic properties [85]. Furthermore, their absorption of NIR light can also be tuned by controlling their size their morphology and their aggregation state. Among the nanostructures studied for PAI, nanorods [85c], nanostars [85d], nanocages [85e], nanovesicles [85f], were developed. The ability of gold nanoparticles to intensify the photoacoustic phenomenon, by shifting the absorption length into the near-IR range, is also mediated by aggregation [85g]. However, it is important to note that some gold-based nanomaterials have poor photothermal stability, which means that they could melt under pulsed laser irradiation and therefore lose their optical absorbance. It is also important to remember that gold-based nanomaterials biodegradability is still a challenge [85h].

Any NIR-absorbing nanosystem can be a candidate contrast agent for PAI, provided it is a poor fluorophore. Thus, upconversion nanoparticles (UCNPs) based on oleic acid stabilized NaY_4: Yb^{3+}: Er^{3+} phosphors made water-dispersible in the presence of cyclodextrin, have proved suitable for PAI [86]. In this case, the enhancement of the photoacoustic signal is based on the combination of the UCNPs' heating capacity and the quenching of their photoluminescence by a non-radiative process.

Carbon-based nanomaterials [87a] such as carbon nanotubes [87b], graphene flakes [87c] but also carbon dots [87d] or hollow carbon-based nanoparticles [87e] have also been developed as contrast agents for PAI. In addition to being easy to manufacture, they have the advantage of having a strong NIR absorption and a high photothermal conversion efficiency. If their absorption coefficient needs to be enhanced, the elaboration of hybrid systems with gold nanomaterials can be considered [87a]. However, special caution should be paid to using carbon nanomaterials, especially long and rigid carbon nanotubes, because of their potential toxicity and their biopersistence [87f].

Two-dimensional transition metal chalcogenides (2D TMC) and dichalcogenides (2D TMDC) nanomaterials whose formulas are respectively MX and MX_2 (where M represents a transition metal from groups IVB to VIIB, and X a chalcogenide typically S, Se and Te) are also of interest for photoacoustic imaging [88]. The most studied TM(*D*)C semi-

conducting materials include copper selenide (CuSe) [88c], tungsten sulfide (WS_2) [88d], molybdenum sulfide (MoS_2) [88e], because of their strong NIR absorption and good photothermal conversion efficacy. The disadvantage of TM(*D*)Cs is that they contain heavy metals and, here again, attention must be paid to their non-degradability, which can lead to deleterious long-term biological effects and, consequently, limit their use in clinical applications.

In addition to PAI contrast agents cited above, black phosphorus (BP) bulk crystals, when exfoliated into single atomic layer-structured nanosheets have been developed for PAI applications [89]. Indeed, these metal-free semi-conducting structures possess tunable energy band gap, compatible with strong absorption in the UV and NIR regions as well as high photothermal conversion properties. In particular, pegylated ultrasmall BP nanoparticles were injected into tumor-bearing mice, and the accumulation of these long-circulating nanoparticles have allowed to discriminate by PAI the tumor from vital organs [89c]. However, the toxicity of BP-based nanosystems to cells is still debated. In particular, the influence of their biodegradation mechanisms and by-products on cells is still poorly understood and has not yet been sufficiently evaluated to allow their safe use *in vivo* [89e].

Organic contrast agents: In parallel with inorganic agents, biocompatible organic dyes have been developed as PAI contrast agents. This category of probes includes molecules and organic nanoparticles. Among the most used molecular dyes are heptamethine-based cyanine dyes (Fig. 7) [90a–e].

Heptamethine cyanine dyes are widely used due to their narrow absorption bands in the NIR range and high molar extinction coefficients, and good photothermal performances. Their photophysical properties can be tuned by modifying the polymethine chain as well as the heterocyclic moieties. Finally, these molecules can be considered as small and easily eliminated from the body. Thus, in the family of heptamethine cyanine dyes, FDA-approved indocyanine green (ICG) [91a], IRDye800CW [91b], (Fig. 8) or AlexaFluor 750 [91c] have been used for PA imaging applications.

ZW800–1 is a heptamethine indocyanine zwitterionic fluorophore that has attracted growing interest for uses in PAI [92]. This biocompatible dye reported by Frangioni's group has been developed as an alternative to ICG since this later is far from being ideal due to its moderate optical properties, its high liver uptake, its non-specific interaction with background tissues, and its instability in aqueous medium. The heptamethine core of ZW800–1 is hydrophobic, and the presence of ammonium and sulfonate groups provides zwitterionic character and water solubility [92a]. Its absorption peak is around 790 nm, in the window of biological transparency. It has a high molar extinction coefficient ($\varepsilon_{788\ nm} = 249{,}000\ L\ mol^{-1}$ in 100 % FBS) as well as a high thermal conversion capacity, and its fluorescence quantum yield is relatively low (15.1 %) [92a].

It should be noted, however, that the aqueous solubility, the photophysical stability, and the half-life in circulation of these organic PAI probes can be improved if they are conveyed within nanocarriers such as micelles [93a–c], liposomes [93d–k] polymersomes [93l], or even proteins [93m–n]. It should also be noted that cyanine probes tend to aggregate in solution, making them poorly soluble and therefore of little interest for *in vivo* applications. However, the formation of aggregates (J-aggregates) is accompanied by a bathochromic shift of absorption wavelengths towards the NIR-II window. Strategies for encapsulating these J-aggregates within micelles, liposomes or polymersomes therefore take advantage of the absorption of aggregated probes beyond 900 nm to significantly enhance the photoacoustic signal. Furthermore, compared to inorganic nanomaterials, nanocarriers doped with these dyes show very good biocompatibility and biodegradability [94].

Among organic systems that exhibit interesting photoacoustic properties, structurally conjugated conductive and semiconductive polymers have been developed as PAI contrast agents. These polymers are characterized by a π-conjugated backbone in which electrons are delocalized by different mechanisms (hopping, tunneling and related mechanisms). They can be designed to have large extinction coefficients, adjustable absorption wavelengths, which results in tunable optical properties, namely high NIR-absorption. They can also be formulated along with amphiphilic polymers or surfactants into nanoparticles with good water dispersibility and biocompatibility [95a–d,h,m]. Different backbones such as, polyfluorene – *co* – thiophen [95a], diketopyrrolopyrrole-dithiophene [95b], indigoid π-conjugated moieties [95c], pyrrolopyrrole [95o], polythiophene-*co*-pyrazine [95i], polydopamine [95l] or backbones based on electron donor-electron acceptor pairs [95d,e,f,j,k,l] have been used. The corresponding conjugated polymers and related nanoparticles exhibit strong absorption in the NIR-I and NIR-II optical windows which favors PAI effect higher than that of gold nanoparticles or carbon nanotubes [96].

In the context of organic systems developed for photoacoustic imaging, melanin nanoparticles cannot be avoided. As previously mentioned, melanin is an endogenous photo-absorber that has no characteristic maximum in the NIR region but demonstrates a broad absorption spectrum that can be activated by any laser wavelength [81]. By mimicking melanin, water-soluble melanin nanoparticles are therefore active systems for photoacoustic imaging [97]. Synthetic melanin nanoparticles are obtained from melanin granules isolated from natural sources [97a], by neutralization of dopamine hydrochloride with sodium hydroxide and spontaneous oxidation of dopamine in air [97b,c], or enzymatic oxidation of precursor molecules such as tyrosine and 3,4-dihydroxy-*L*-phenylalanine [97b].

Water solubility can be improved by pegylation [97e]. Melanin nanoparticle surface can also be designed to amplify the PA signal strength by aggregation [97c], to promote condensation with nucleic acids [97f] or to target specific angiogenesis receptors [97j].

The native biocompatibility of melanin is maintained in all categories of melanin-like nanoparticles since they exhibit low or minor toxicity [97i]. They can also be used as delivery systems thanks to encapsulation or grafting drugs strategies to provide interesting theranostic solutions [97k].

4. Bimodal MRI-PAI imaging

To meet resolution and sensitivity requirements, combinations of techniques possessing these two characteristics are currently being developed. Of the various imaging modalities mentioned above, MRI is one of the most widely used in medical imaging, thanks to its excellent resolution and lack of penetration depth limits. To compensate for its

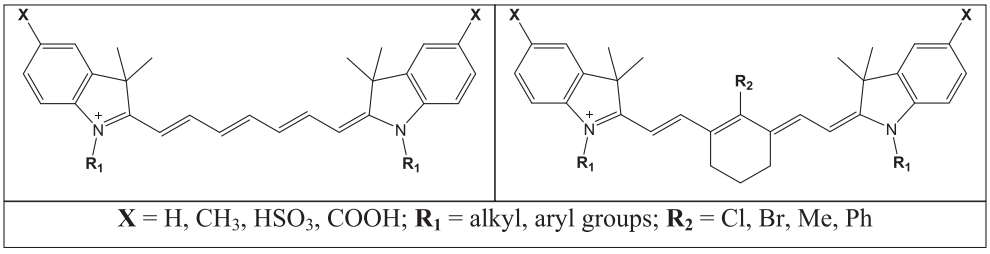

Fig. 7. Prototype of heptamethine cyanine dyes: general structures.

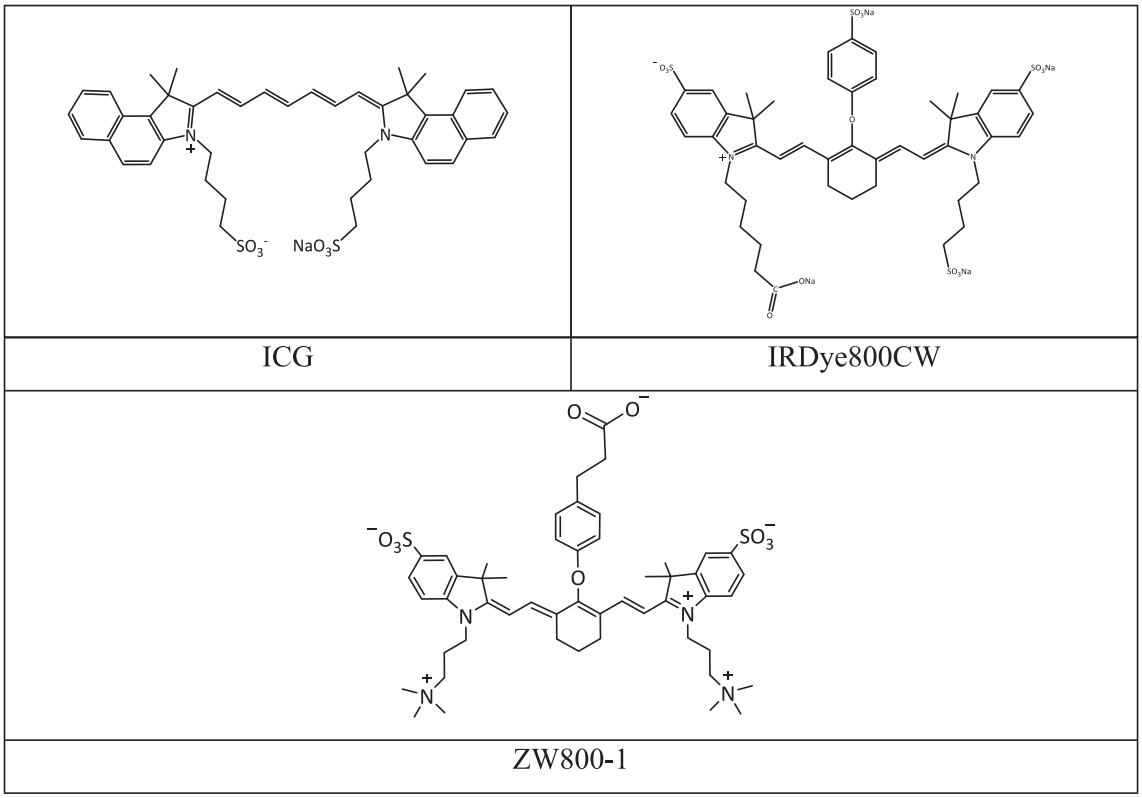

Fig. 8. Examples of PAI organic dyes.

lack of sensitivity, the solution is to combine MRI with another imaging modality with good sensitivity. Tandem MRI-OI, MRI-PET, and MRI-SPECT imaging modalities are already in use. The use of non-ionizing radiation is recommended for patient health, doctors, and nursing staff. This is why the combination of MRI with optical imaging can be favored over nuclear imaging. Despite its very high sensitivity, OI does not penetrate biological tissue very deeply, even using NIR emission (which allows penetration depths of up to up to 2 cm), and spatial resolution is poor because of photon scattering. This is where PA imaging comes in, because as previously said, this non-ionizing technique has a good sensitivity a better penetration depth, and a far finer depth localization [79e]. The creation of a bimodal MRI-PAI probe would therefore make it possible to combine the good resolution of MRI with the sensitivity of PAI [98a,b]. Various approaches to combine the two imaging modalities have been reported. In the following, we provide a non-exhaustive list of what exists in the literature and present a few examples. One solution is to take advantage of the ability of certain constituents, such as europium, to exhibit bimodal MRI/PAI behavior [99]. The mode of action of these probes is based on the redox-responsive nature of Eu and the difference in the properties between Eu in the +2 and + 3 oxidation states. Thus, Eu in the +2 oxidation state is active in T_1-weighted magnetic resonance imaging and also in photoacoustic imaging, while Eu in the +3 oxidation state is inactive in both imaging modes. That said, although the design of this type of bimodal probe is straightforward, their biocompatibility in living systems remains a major concern. A second solution is to combine the two separate imaging functions in a single unit. To this end, two approaches, molecular and nanoparticulate, have been developed. An example of a molecular probe is the combination of the Gd-PCTA complex and the ZW800–1 chromophore on a L-lysine backbone [100]. MR and PA phantom images illustrate the appearance of contrast in both imaging modalities. Probably more widespread is the combination of the two imaging functionalities *via* the nanoparticle pathway. Several approaches have been developed for this purpose. The first approach, which bridges the gap between the molecular and nanoparticle aspects, involves combining a gadolinium chelate for MRI imaging and a near-IR chromophore (triazole IR780) within a molecular platform. The resulting Gd-IR780 entity then evolves in apoptotic tumor cells into a macrocyclic Gd-IR780MC form that can self-assemble *in vivo* as Gd-IR780-NPs nanoparticles. In this form, a strong aggregation-caused quenching (ACQ) effect helps to enhance the PA signal of IR780 probe, and restrict molecular rotation of Gd chelate which results in r_1 relaxivity enhancement [101].

The following approaches involve developing bimodal inorganic/inorganic or hybrid inorganic/organic MRI/PAI nanoparticles.

In the first category, both MRI and PAI functionalities are provided by inorganic components [102]. Prussian-Blue (PB) nanoprobe has thus been developed for this goal [102a], PB combining both MRI and PAI properties. This iron-based probe proved to be responsive to redox stimuli, particularly in the presence of $ONOO^-$, its MRI and PAI efficiencies being exalted. Cobalt core/carbon shell or cobalt core/gold shell-based nanoparticles with both magnetization and light absorption properties were also described [102b,c]. In these probes, ferromagnetic cobalt particles that provide magnetization and T_2-weighted MR images were coated with a carbon or a gold shell for either PA imaging and biocompatibility. Alongside these combinations, most functional associations make extensive use of iron oxide-based magnetic nanoparticles. Fe_3O_4 superparamagnetic nanoparticles provide T_2-MRI contrast or according to the magnetic core size a T_1-T_2 double-contrast while PA modality is ensured by gold nanoparticles within magneto-plasmonic Janus vesicles [102d], MnO_2 nanostructures [102e], Fe_3O_4 itself [102f], or Cu_2O whose near-IR absorption and therefore PA signal are greatly enhanced by sulfidization in the presence of endogenous H_2S in colon cancer tumors [102g].

In the second category, one of the two functionalities is provided by an organic or organometallic component [103]. Bimodal contrast agents were developed by association of conjugated polymers with iron oxide nanoparticles using an amphiphilic polymer [103a]. This combination enhances the photoacoustic activity of the conjugated polymer part

(compared with the version in the absence of a superparamagnetic agent), while preserving the intact MRI action of the iron oxide nanoparticles. ICG-coated superparamagnetic iron oxide nanoparticle clusters [103b] or association of iron oxide and gold nanoparticles coated with a layer of silver nanoparticles and covalently conjugated with IRDye800RS [103c] have also been designed to be detected in T_2 MRI and PAI in real-time. They were also used in a surgical resection model for PA-guided surgery. In several nanoparticle structures, the paramagnetic ions commonly used in MRI contrast agents have been integrated into nanoparticles in their ionic form. Gd(III) or Mn(II) ions were thus trapped within melanin nanoparticles leading to T_1-MRI and PAI bimodal probe [103d,e]. Multi-layered up-converting nanoparticles with a $NaGdF_4$ shell and ICG surface functionalization were developed to provide access to high-quality MRI and PAI images [103f]. Gd(III) can also be introduced as the $[GdO]^+$ cation in sulfonate based saline $[GdO]^+[ICG]^-$ nanoparticles [103g]. Gadolinium ions were also incorporated in the form of Gd chelates (GdDTPA) into nanoparticles and associated with bismuth nanoparticles [103h]. Probably more securely, they were also encapsulated as chelates (GdDOTA) in nanogels of hyaluronic acid, and chitosan functionalized with ZW800 as PAI probe [103i]. In the latter systems, encapsulation of gadolinium chelates in a hydrophilic matrix considerably amplifies their MRI signal [103i]. Similarly, grafting ZW800 to the hydrogel matrix enhances its PAI signal. As already described for MRI contrast agents, the use of biocompatible hydrogel structures is proving to be an attractive solution for bringing together complementary imaging modalities such as MRI and PAI imaging, while also amplifying the corresponding contrasts when compared with those obtained by individual probes.

5. Conclusion

The vast array of imaging techniques and contrast agents available to the preclinical and medical worlds enables us to acquire the anatomical and functional information needed for diagnosis. Each imaging modality necessitates the utilization of a contrast agent, either to optimize its performance (*e.g.*, X-ray, MRI, US) or because, without a contrast agent, the modality is rendered ineffective, as the signal detecting the pathological zone is emitted by the injected exogenous probe (*e.g.*, SPECT, PET, OI, PAI). A review of the specific characteristics of each technique is summarized in the table below (Table 1). Clearly, no single technique can meet all the necessary criteria in terms of resolution, sensitivity and depth of penetration. With regard to sensitivity, the most effective techniques are unquestionably SPECT, PET and optical and photoacoustic imaging. However, SPECT and PET have the disadvantage of exposing patients and medical staff to radiation and optical methods suffer from low spatial resolution (OI) and penetration depth (PAI). About spatial resolution, MRI, X-ray, and ultrasound are the most effective techniques but MRI, without the use of contrast agents, is relatively insensitive, while X-ray has the same drawbacks than SPECT and PET nuclear imaging techniques. Finally, from the point of view of deep tissue imaging, X-ray imaging, MRI, SPECT and PET have no limits in terms of penetration depth, unlike, for example, optical methods which, depending on the wavelength, are subject to limitations imposed by the diffraction of photons by tissues. Thus, the quest for earlier and more accurate diagnosis, coupled with the growing need for image-guided surgery, implies that imaging strategies based on a combination of complementary techniques must be developed.

Therefore, from a chemical point of view, this is accompanied by the development of single or multi-modal molecular or nanoparticulate

Table 1
Imaging modalities at a glance.

X-rays
Sensitivity: $10^{-2} – 10^{-4}$ mol.L^{-1}
Spatial resolution : < 20 µm
Penetration depth : no limit
Drawback : radiation exposure

SPECT
Sensitivity: 10^{-10} mol.L^{-1}
Spatial resolution : 0.5 – 1 mm
Penetration depth : no limit
Drawback : radiation exposure

MRI
Sensitivity: $10^{-3} – 10^{-5}$ mol.L^{-1}
Spatial resolution : 25 – 100 µm
Penetration depth : no limit
Drawback : low sensitivity

PET
Sensitivity: $10^{-11} – 10^{-12}$ mol.L^{-1}
Spatial resolution : 1 – 2 mm
Penetration depth : no limit
Drawback : radiation exposure

ULTRASOUNDS
Sensitivity: 10^{-8} mol.L^{-1}
Spatial resolution : 50 – 500 µm
Penetration depth : mm - cm
Drawback : low penetration depth

OPTICAL IMAGING
Sensitivity: 10^{-12} mol.L^{-1}
Spatial resolution : 1 – 5 mm
Penetration depth : 1 - 2 mm
Drawback : low spatial resolution

PAI
Sensitivity: $10^{-9} – 10^{-12}$ mol.L^{-1}
Spatial resolution : 50 – 500 µm
Penetration depth : < 5 cm
Drawback : poor tissue penetration at short wavelength

contrast agents, tailored to the desired imaging modalities. In particular, this review shows that a wide variety of nanoparticle probes that improve not only the performances of conventional contrast agents but also their pharmacological properties can be envisaged.

The next step is to develop nanoparticles able to deliver imaging agents to a specific target *in vivo*. As stated in the introduction, our intention was not to provide an overview of the field of targeted nanoparticles for imaging. Still, we can provide some key points to consider so that these probes can hit their target, improve image accuracy, and be low or non-toxic. For imaging purposes, nanoparticles do not need to penetrate deep into tissues but rapidly detect the relevant target sites while minimizing off-target recognition, and then be eliminated from the body *via* renal clearance.

While the dual criteria of resolution and sensitivity must be met, validation of targets that play a critical role in disease, identification of candidates with high affinity and adsorption at the target site, evaluation of the dose required for a high signal-to-noise ratio, and low potential toxicity are essential considerations. In other words, to get from the laboratory to the patient's bedside, these targeted nanoparticles need to provide unique information that is impossible to obtain through other ways, and their route of administration must be similar to that of conventional imaging products [104a]. The intravenous administration of imaging agents is a standard procedure, and this will also apply to the nanoparticles under discussion.

The biodistribution of nanoparticles is influenced by their size, geometry, charge, and surface modification [104b]. A compromise must be found in terms of size, given that nanoparticles smaller than 10 nm are rapidly eliminated by the kidneys, while those larger than or equal to 300 nm are rapidly taken up by mononuclear phagocytic cells [104c]. In the case of intravenous administration, a major limitation to their delivery and targeting is their opsonization and their recognition by the reticuloendothelial system [104d]. To overcome this drawback, nanoparticle coatings should be considered, PEGylation being one of the most developed until now. The grafting of poly(ethyleneglycol)s, particularly those with a molecular weight of at least 2000 Da, induces the formation of a hydrating layer at the nanoparticle surface which hinders the adsorption of proteins. In order not to compromise the exposure of targeting ligands to cell receptors, PEG coverage must be sufficiently low for the PEG chains to adopt mushroom-shaped conformations. A probably more satisfactory solution would be to install the targeting ligand to the end of PEG chains with higher grafting densities to favor brush-like conformations and ensure good presentation of the ligands to the receptors to be targeted [104d]. However, this solution is not without drawbacks, as it is well known that when PEGylated nanoparticles are repeatedly administered, they can lose their long-circulation properties due to an accelerated blood clearance phenomenon [104e]. Alternatives such as poly(ethyl ethylene phosphate)s [104f], zwitterionic polymers [104g] or coatings that can incorporate peptide mimetics capable of preventing phagocytosis by macrophages [104h] are conceivable prospects.

Prior to their utilization in clinical applications, it is imperative that the biosafety of nanoparticles is given due consideration. Oxidative stress and reactive oxygen species production, inflammation, mitochondrial dysfunction and DNA damage as well as cellular uptake and possible nanoparticle internalization must be subjected to rigorous *in vitro* evaluation [104i]. Although these assessments are readily available, they only very partially reflect the *in vivo* toxicity of nanoparticles. The biodistribution and clearance of nanoparticles offer insights into their localization, retention, and metabolism. Furthermore, analysis of animal's blood composition and identification of histological modifications of specific cells, tissues, or organs induced by the exposition of animals to nanoparticles provide a valuable indication of the toxicity of nanoparticles. Finally, acute toxicity and long-term toxicity tests are important reference points in the preclinical assessment of nanoparticle safety [104i]. Although the animal models used for these assessments are physiologically different from humans, these studies allow the most appropriate systems to be selected before clinical trials.

In the meantime, we believe that developing systems using (i) active substances already approved by international medicines agencies and (ii) materials and solvents recognised for their long-term biocompatibility and bioresorbability, is probably the medium-term path to follow.

Authors' Contribution

Camille Gosée did the bibliographical research for the document and wrote the first versions of the manuscript. Juliette Moreau and Céline Henoumont took part in the literature search on MR imaging agents and reviewed this part of the manuscript. Juliette Moreau took part in the literature search on optical imaging agents and reviewed this part of the manuscript. Maite Callewaert and Christelle Kowandy took part in the literature search on nanoparticle imaging agents and reviewed the part of the manuscript dedicated to nanoparticles for MRI. Lionel Larbanoix supervised bibliographic research on photoacoustic imaging. Sophie Laurent was instrumental in finding the necessary funding for the study and participated in the proofreading process. Françoise Chuburu also helped find the necessary funding, and, with Cyril Cadiou, supervised the entire bibliographical study and drafting of the manuscript.

Declaration of competing interest

The authors declare the following financial interests/personal relationships which may be considered as potential competing interests: Chuburu reports financial support was provided by Programme de cooperation transfrontalière Interreg France-Wallonie-Vlaanderen. Reports a relationship with that includes. Has patent pending to. If there are other authors, they declare that they have no known competing financial interests or personal relationships that could have appeared to influence the work reported in this paper.

Acknowledgments

The project leading to this publication has received funding from Université de Reims Champagne-Ardenne and Université de Mons (Camille Gosée PhD fellowship). The authors would like to thank the "Programme de cooperation transfrontalière Interreg France-Wallonie-Vlaanderen" for its support through the "Nanocardio" project, and Nano'Mat and PlAneT platforms (supported by the European Regional Development Fund and the Region Champagne Ardenne). The CMMI and its bioprofiling platform would like to thank the European Regional Development Fund and the Walloon Region for their financial support.

Data availability

Data will be made available on request.

References

[1] A. Walter, P. Paul-Gilloteaux, B. Plochberger, L. Sefc, P. Verkade, J.G. Mannheim, P. Slezak, A. Unterhuber, M. Marchetti-Deschmann, M. Ogris, K. Bühler, D. Fixler, S.H. Geyer, W.J. Weninger, M. Glösmann, S. Handschuh, T. Wanek, Correlated multimodal imaging in life sciences: expanding the biomedical horizon, Front. Phys. 8 (2020), https://doi.org/10.3389/fphy.2020.00047.

[2] (a) I. Vermeulen, E.M. Isin, P. Barton, B. Cillero-Pastor, R.M.A. Heeren, Multimodal molecular imaging in drug discovery and development, Drug Discov. Today 27 (2022) 2086–2099, https://doi.org/10.1016/j.drudis.2022.04.009;
(b) S. Manohar, S.S. Gambhir, Clinical photoacoustic imaging, Photoacoustics 19 (2020) 100196, https://doi.org/10.1016/j.pacs.2020.100196.

[3] D.W. Townsend, Dual-modality imaging: combining anatomy and function, J. Nucl. Med. 49 (2008) 938–955, https://doi.org/10.2967/jnumed.108.051276.

[4] X. Li, X.-N. Zhang, X.-D. Li, J. Chang, X. Li, X.-N. Zhang, X.-D. Li, J. Chang, Multimodality imaging in nanomedicine and nanotheranostics, Cancer Biol. Med. 13 (2016) 339–348, https://doi.org/10.20892/j.issn.2095-3941.2016.0055.

[5] (a) R.F. Mould, The Early History of X-ray diagnosis with emphasis on the contributions of physics 1895-1915, Phys. Med. Biol. 40 (1995) 1741–1787, https://doi.org/10.1088/0031-9155/40/11/001;
(b) X. Ou, X. Chen, X. Xu, L. Xie, X. Chen, Z. Hong, H. Bai, X. Liu, Q. Chen, L. Li,

H. Yang, Recent development in X-Ray imaging technology: future and challenges, AAAS Research (2021) 9892152, https://doi.org/10.34133/2021/9892152.
[6] A. Sudhyadhom, On the molecular relationship between Hounsfield Unit (HU), mass density, and electron density in computed tomography (CT), PLoS One 15 (2020) e0244861, https://doi.org/10.1371/journal.pone.0244861.
[7] (a) J. Wallyn, N. Anton, S. Akram, T.F. Vandamme, Biomedical imaging: principles, technologies, clinical aspects, contrast agents, limitations and future trends in nanomedicines, Pharm. Res. 36 (2019) 78, https://doi.org/10.1007/s11095-019-2608-5;
(b) H. Lusic, M.W. Grinstaff, X-ray-computed tomography contrast agents, Chem. Rev. 113 (2013) 1641–1666, https://doi.org/10.1021/cr200358s.
[8] M. Pease, D. Arefan, J. Barber, E. Yuh, A. Puccio, K. Hochberger, E. Nwachuku, S. Roy, S. Casillo, N. Temkin, D.O. Okonkwo, S. Wu, N. Badjatia, Y. Bodien, A.-C. Duhaime, V.R. Feeser, A.R. Ferguson, B. Foreman, R. Gardner, S. Gopinath, C. D. Keene, C. Madden, M. McCrea, P. Mukherjee, L.B. Ngwenya, D. Schnyer, S. Taylor, J.K. Yue, Outcome prediction in patients with severe traumatic brain injury using deep learning from head CT scans, Radiology 304 (2022) 385–394, https://doi.org/10.1148/radiol.212181.
[9] I. Shafi, S. Din, A. Khan, I.D.L.T. Díez, R. Del J.P. Casanova, K.T. Pifarre, I. Ashraf, An Effective method for lung cancer diagnosis from CT scan using deep learning-based support vector network, Cancers (Basel) 14 (2022) 5457, https://doi.org/10.3390/cancers14215457.
[10] M.M. Koç, N. Aslan, A.P. Kao, A.H. Barber, Evaluation of X-ray tomography contrast agents: a review of production, protocols, and biological applications, Microsc. Res. Tech. 82 (2019) 812–848, https://doi.org/10.1002/jemt.23225.
[11] B.M. Yeh, P.F. FitzGerald, P.M. Edic, J.W. Lambert, R.E. Colborn, M.E. Marino, P. M. Evans, J.C. Roberts, Z.J. Wang, M.J. Wong, P.J. Bonitatibus, Opportunities for new CT contrast agents to maximize the diagnostic potential of emerging spectral CT technologies, Adv. Drug Deliv. Rev. 113 (2017) 201–222, https://doi.org/10.1016/j.addr.2016.09.001.
[12] (a) N. Lee, S.H. Choi, T. Hyeon, Nano-Sized CT contrast agents, Adv. Mater. 25 (2013) 2641–2660, https://doi.org/10.1002/adma.201300081;
(b) N. Aslan, B. Ceylan, M.M. Koç, F. Findik, Metallic nanoparticles as X-Ray computed tomography (CT) contrast agents: a review, J. Mol. Struct. 1219 (2020) 128599, https://doi.org/10.1016/j.molstruc.2020.128599.
[13] Y.C. Dong, M. Hajfathalian, P.S.N. Maidment, J.C. Hsu, P.C. Naha, S. Si-Mohamed, M. Breuilly, J. Kim, P. Chhour, P. Douek, H.I. Litt, D.P. Cormode, Effect of gold nanoparticle size on their properties as contrast agents for computed tomography, Sci. Rep. 9 (2019) 14912, https://doi.org/10.1038/s41598-019-50332-8.
[14] J. Liu, X. Zheng, L. Yan, L. Zhou, G. Tian, W. Yin, L. Wang, Y. Liu, Z. Hu, Z. Gu, C. Chen, Y. Zhao, Bismuth sulfide nanorods as a precision nanomedicine for in vivo multimodal imaging-guided photothermal therapy of tumor, ACS Nano 9 (2015) 696–707, https://doi.org/10.1021/nn506137n.
[15] (a) C. Cruje, J. Dunmore-Buyze, J.P. MacDonald, D.W. Holdsworth, M. Drangova, E.R. Gillies, Polymer assembly encapsulation of lanthanide nanoparticles as contrast agents for in vivo micro-CT, Biomacromolecules 19 (2018) 896–905, https://doi.org/10.1021/acs.biomac.7b01685;
(b) E.N.M. Cheung, R.D.A. Alvares, W. Oakden, R. Chaudhary, M.L. Hill, J. Pichaandi, G.C.H. Mo, C. Yip, P.M. Macdonald, G.J. Stanisz, F.C.J.M. van Veggel, R.S. Prosser, Polymer-stabilized lanthanide fluoride nanoparticle aggregates as contrast agents for magnetic resonance imaging and computed tomography, Chem. Mater. 22 (2010) 4728–4739, https://doi.org/10.1021/cm101036a;
(c) S. He, N.J.J. Johnson, V.A. Nguyen Huu, E. Cory, Y. Huang, R.L. Sah, J. V. Jokerst, A. Almutairi, Simultaneous enhancement of photoluminescence, MRI relaxivity, and ct contrast by tuning the interfacial layer of lanthanide heteroepitaxial nanoparticles, Nano Lett. 17 (2017) 4873–4880, https://doi.org/10.1021/acs.nanolett.7b01753;
(d) H. Xing, W. Bu, Q. Ren, X. Zheng, M. Li, S. Zhang, H. Qu, Z. Wang, Y. Hua, K. Zhao, L. Zhou, W. Peng, J. Shi, A $NaYbF_4$: tm^{3+} nanoprobe for CT and NIR-to-NIR fluorescent bimodal imaging, Biomaterials 33 (2012) 5384–5393, https://doi.org/10.1016/j.biomaterials.2012.04.002.
[16] (a) P.G. Newman, G.S. Rozycki, The history of ultrasound, Surg. Clin. North Am. 78 (1998) 179–195, https://doi.org/10.1016/S0039-6109(05)70308-X;
(b) J. Osterwalder, E. Polyzogopoulou, B. Hoffmann, Point-of-Care ultrasound—history, current and evolving clinical concepts in emergency medicine, Medicina 59 (2023) 2179, https://doi.org/10.3390/medicina59122179.
[17] J.E. Aldrich, Basic physics of ultrasound imaging, Crit. Care Med. 35 (2007) S131–S137, https://doi.org/10.1097/01.CCM.0000260624.99430.22.
[18] R. Gramiak, P.M. Shah, Echocardiography of the aortic root, Investig. Radiol. 3 (1968) 356–366, https://doi.org/10.1097/00004424-196809000-00011.
[19] M.A. Borden, K.-H. Song, Reverse engineering the ultrasound contrast agent, Adv. Colloid Interf. Sci. 262 (2018) 39–49, https://doi.org/10.1016/j.cis.2018.10.004.
[20] (a) J.R. Lindner, Microbubbles in medical imaging: current applications and future directions, Nat. Rev. Drug Discov. 3 (2004) 527–533, https://doi.org/10.1038/nrd1417;
(b) P. Frinking, T. Segers, Y. Luan, F. Tranquart, Three decades of ultrasound contrast agents: a review of the past, present and future improvements, Ultrasound Med. Biol. 46 (2020) 892–908, https://doi.org/10.1016/j.ultrasmedbio.2019.12.008;
(c) Y. Wang, H. Cong, S. Wang, B. Yu, Y. Shen, Development and application of ultrasound contrast agents in biomedicine, J. Mater. Chem. B 9 (2021) 7633–7661, https://doi.org/10.1039/D1TB00850A.
[21] T. Segers, P. Kruizinga, M.P. Kok, G. Lajoinie, N. de Jong, M. Versluis, Monodisperse versus polydisperse ultrasound contrast agents: non-linear response, sensitivity, and deep tissue imaging potential, Ultrasound Med. Biol. 44 (2018) 1482–1492, https://doi.org/10.1016/j.ultrasmedbio.2018.03.019.
[22] (a) B.A. Kaufmann, J.R. Lindner, Molecular imaging with targeted contrast ultrasound, Curr. Opin. Biotechnol. 18 (2007) 11–16, https://doi.org/10.1016/j.copbio.2007.01.004;
(b) J. Wischhusen, F. Padilla, Ultrasound molecular imaging with targeted microbubbles for cancer diagnostics: from bench to bedside, IRBM 40 (2019) 3–9, https://doi.org/10.1016/j.irbm.2018.10.007;
(c) S.A.G. Langeveld, B. Meijlink, K. Kooiman, Phospholipid-coated targeted microbubbles for ultrasound molecular imaging and therapy, Curr. Opin. Chem. Biol. 63 (2021) 171–179, https://doi.org/10.1016/j.cbpa.2021.04.013;
(d) S. Wang, J.A. Hossack, A.L. Klibanov, Targeting of microbubbles: contrast agents for ultrasound molecular imaging, J. Drug Target. 26 (2018) 420–434, https://doi.org/10.1080/1061186X.2017.1419362.
[23] (a) R. Xiong, R.X. Xu, C. Huang, S. De Smedt, K. Braeckmans, Stimuli-responsive nanobubbles for biomedical applications, Chem. Soc. Rev. 50 (2021) 5746–5776, https://doi.org/10.1039/C9CS00839J;
(b) X. Cui, X. Han, L. Yu, B. Zhang, Y. Chen, Intrinsic chemistry and design principle of ultrasound-responsive nanomedicine, Nano Today 28 (2019) 100773, https://doi.org/10.1016/j.nantod.2019.100773.
[24] T.M. Krupka, L. Solorio, R.E. Wilson, H. Wu, N. Azar, A.A. Exner, Formulation and Characterization of echogenic lipid−pluronic nanobubbles, Mol. Pharm. 7 (2010) 49–59, https://doi.org/10.1021/mp9001816.
[25] N. Rapoport, K.-H. Nam, R. Gupta, Z. Gao, P. Mohan, A. Payne, N. Todd, X. Liu, T. Kim, J. Shea, C. Scaife, D.L. Parker, E.-K. Jeong, A.M. Kennedy, Ultrasound-mediated tumor imaging and nanotherapy using drug loaded, block copolymer stabilized perfluorocarbon nanoemulsions, J. Control. Release 153 (2011) 4–15, https://doi.org/10.1016/j.jconrel.2011.01.022.
[26] (a) Y. Endo-Takahashi, Y. Negishi, Microbubbles and nanobubbles with ultrasound for systemic gene delivery, Pharmaceutics 12 (2020) 964, https://doi.org/10.3390/pharmaceutics12100964;
(b) D. Park, H.C. Jung, J. Park, S. Bae, U. Shin, S.W. Kim, C.W. Kim, Y.H. Lee, J. Seo, Synthesis of echogenic liposomes for sonoporation, Micro Nano Lett. 17 (2022) 276–285, https://doi.org/10.1049/mna2.12133.
[27] (a) A. Viard, F. Eustache, S. Segobin, History of magnetic resonance imaging: a trip down memory lane, Neuroscience 474 (2021) 3–13, https://doi.org/10.1016/j.neuroscience.2021.06.038;
(b) C. de Haën, Conception of the first magnetic resonance imaging contrast agents: a brief history, Top. Magn. Reson. Imaging 12 (2001) 221–230, https://doi.org/10.1097/00002142-200108000-00002;
(c) R.J. Macchia, J.E. Termine, C.D. Buchen, Raymond V. Damadian, M.D.: magnetic resonance imaging and the controversy of the 2003 Nobel prize in physiology or medicine, J. Urol. 178 (2007) 783–785, https://doi.org/10.1016/j.juro.2007.05.019.
[28] C. Westbrook, Handbook of MRI technique, Wiley-Blackwell, 2022.
[29] B. Doan, S. Meme, J. Beloeil, General principles of MRI, in, Chem. Contrast Agents Med. Magn. Reson. Imaging, Wiley (2013) 1–23, https://doi.org/10.1002/9781118503652.ch1.
[30] J.P. Wansapura, S.K. Holland, R.S. Dunn, W.S. Ball, NMR relaxation times in the human brain at 3.0 tesla, J. Magn. Reson. Imaging 9 (1999) 531–538, https://doi.org/10.1002/(SICI)1522-2586(199904)9:4<531::AID-JMRI4>3.0.CO;2-L.
[31] M. Port, J.-M. Idée, C. Medina, C. Robic, M. Sabatou, C. Corot, Efficiency, thermodynamic and kinetic stability of marketed gadolinium chelates and their possible clinical consequences: a critical review, BioMetals 21 (2008) 469–490, https://doi.org/10.1007/s10534-008-9135-x.
[32] S. Laurent, D. Forge, M. Port, A. Roch, C. Robic, L. Vander Elst, R.N. Muller, Magnetic iron oxide nanoparticles: synthesis, stabilization, vectorization, physicochemical characterizations, and biological applications, Chem. Rev. 108 (2008) 2064–2110, https://doi.org/10.1021/cr068445e.
[33] (a) J. Wahsner, E.M. Gale, A. Rodríguez-Rodríguez, P. Caravan, Chemistry of MRI contrast agents: current challenges and new frontiers, Chem. Rev. 119 (2019) 957–1057, https://doi.org/10.1021/acs.chemrev.8b00363;
(b) European Medecines Agency. Gadolinium-containing contrast agents. EMA/424715/2017, 2025.
[34] (a) A. Som, J.-G. Rosenboom, A. Chandler, R.A. Sheth, E. Wehrenberg-Klee, Image-guided intratumoral immunotherapy: developing a clinically practical technology, Adv. Drug Deliv. Rev. 189 (2022) 114505, https://doi.org/10.1016/j.addr.2022.114505;
(b) F. Mahmood, U.G. Nielsen, C.B. Jørgensen, C. Brink, H.S. Thomsen, R. H. Hansen, Safety of gadolinium based contrast agents in magnetic resonance imaging-guided radiotherapy – An investigation of chelate stability using relaxometry, Phys. Imaging Radiat. Oncol. 21 (2022) 96–100, https://doi.org/10.1016/j.phro.2022.02.015.
[35] (a) M. Le Fur, P. Caravan, The biological fate of gadolinium-based MRI contrast agents: a call to action for bioinorganic chemists, Metallomics 11 (2019) 240–254, https://doi.org/10.1039/C8MT00302E;
(b)I.B. Boehm, Classification of gadolinium-based contrast agents (GBCAs)-adverse reactions, Magn. Reson. Imaging 85 (2022) 1–2. doi:https://doi.org/10.1016/j.mri.2021.10.006;. (c) S. Lange, W. Mędrzycka-Dąbrowska, K. Zorena, S. Dąbrowski, D. Ślęzak, A. Malecka-Dubiela, P. Rutkowski, Nephrogenic systemic fibrosis as a complication after gadolinium-containing contrast agents: a rapid review, Int. J. Environ. Res. Public Health 18 (2021) 3000, https://doi.org/10.3390/ijerph18063000;
(d) E. Gianolio, P. Bardini, F. Arena, R. Stefania, E. Di Gregorio, R. Iani, S. Aime,

Gadolinium retention in the rat brain: assessment of the amounts of insoluble gadolinium-containing species and intact gadolinium complexes after repeated administration of gadolinium-based contrast agents, Radiology 285 (2017) 839–849, https://doi.org/10.1148/radiol.2017162857.

[36] (a) C. Robic, M. Port, O. Rousseaux, S. Louguet, N. Fretellier, S. Catoen, C. Factor, S. Le Greneur, C. Medina, P. Bourrinet, I. Raynal, J.-M. Idée, C. Corot, Physicochemical and pharmacokinetic profiles of gadopiclenol, Investig. Radiol. 54 (2019) 475–484, https://doi.org/10.1097/RLI.0000000000000563;
(b) J. Ru, W. Xu, M. Kou, H. Dong, X. Tang, Y. Chen, L. Kang, L. Dai, C. Liang, A novel Gd^{3+} DTPA-bisamide complex with high relaxivity as an MRI contrast agent, J. Mater. Chem. B 11 (2023) 7182–7189, https://doi.org/10.1039/D3TB00720K.

[37] (a) E.M. Gale, I.P. Atanasova, F. Blasi, I. Ay, P. Caravan, A manganese alternative to gadolinium for mri contrast, J. Am. Chem. Soc. 137 (2015) 15548–15557, https://doi.org/10.1021/jacs.5b10748;
(b) A. Forgács, R. Pujales-Paradela, M. Regueiro-Figueroa, L. Valencia, D. Esteban-Gómez, M. Botta, C. Platas-Iglesias, Developing the family of picolinate ligands for Mn^{2+} complexation, Dalton Trans. 46 (2017) 1546–1558, https://doi.org/10.1039/C6DT04442E;
(c) D. Ndiaye, M. Sy, A. Pallier, S. Même, I. de Silva, S. Lacerda, A.M. Nonat, L. J. Charbonnière, É. Tóth, unprecedented kinetic inertness for a mn^{2+} -bispidine chelate: a novel structural entry for mn^{2+} -based imaging agents, Angew. Chem. Int. Ed. 59 (2020) 11958–11963, https://doi.org/10.1002/anie.202003685;
(d) Z. Garda, E. Molnár, N. Hamon, J.L. Barriada, D. Esteban-Gómez, B. Váradi, V. Nagy, K. Pota, F.K. Kálmán, I. Tóth, N. Lihi, C. Platas-Iglesias, É. Tóth, R. Tripier, G. Tircsó, Complexation of Mn(II) by rigid pyclen diacetates: equilibrium, kinetic, relaxometric, density functional theory, and superoxide dismutase activity studies, Inorg. Chem. 60 (2021) 1133–1148, https://doi.org/10.1021/acs.inorgchem.0c03276;
(e) M. Devreux, C. Henoumont, F. Dioury, S. Boutry, O. Vacher, L. Vander Elst, M. Port, R.N. Muller, O. Sandre, S. Laurent, Mn^{2+} Complexes with pyclen-based derivatives as contrast agents for magnetic resonance imaging: synthesis and relaxometry characterization, Inorg. Chem. 60 (2021) 3604–3619, https://doi.org/10.1021/acs.inorgchem.0c03120;
(f) G. Reale, F. Calderoni, T. Ghirardi, F. Porto, F. Illuminati, L. Marvelli, P. Martini, L. Uccelli, E. Tonini, L. Del Bianco, F. Spizzo, M. Capozza, E. Cazzola, A. Carnevale, M. Giganti, A. Turra, J. Esposito, A. Boschi, Development and evaluation of the magnetic properties of a new manganese (ii) complex: a potential MRI contrast agent, Int. J. Mol. Sci. 24 (2023) 3461, https://doi.org/10.3390/ijms24043461;
(g) A. Gupta, P. Caravan, W.S. Price, C. Platas-Iglesias, E.M. Gale, Applications for transition-metal chemistry in contrast-enhanced magnetic resonance imaging, Inorg. Chem. 59 (2020) 6648–6678, https://doi.org/10.1021/acs.inorgchem.0c00510;
(h) C. Henoumont, M. Devreux, S. Laurent, Mn-based MRI contrast agents: an overview, Molecules 28 (2023) 7275, https://doi.org/10.3390/molecules28217275.

[38] (a) E.M. Snyder, D. Asik, S.M. Abozeid, A. Burgio, G. Bateman, S.G. Turowski, J. A. Spernyak, J.R. Morrow, A class of Fe III macrocyclic complexes with alcohol donor groups as effective T1 MRI contrast agents, Angew. Chem. Int. Ed. 59 (2020) 2414–2419, https://doi.org/10.1002/anie.201912273;
(b) D. Asik, R. Smolinski, S.M. Abozeid, T.B. Mitchell, S.G. Turowski, J. A. Spernyak, J.R. Morrow, Modulating the properties of Fe(III) macrocyclic MRI contrast agents by appending sulfonate or hydroxyl groups, Molecules 25 (2020) 2291, https://doi.org/10.3390/molecules25102291;
(c) D. Asik, S.M. Abozeid, S.G. Turowski, J.A. Spernyak, J.R. Morrow, Dinuclear Fe(III) hydroxypropyl-appended macrocyclic complexes as MRI probes, Inorg. Chem. 60 (2021) 8651–8664, https://doi.org/10.1021/acs.inorgchem.1c00634;
(d) L. Palagi, E. Di Gregorio, D. Costanzo, R. Stefania, C. Cavallotti, M. Capozza, S. Aime, E. Gianolio, $Fe(deferasirox)_2$: an iron(III)-based magnetic resonance imaging T1 contrast agent endowed with remarkable molecular and functional characteristics, J. Am. Chem. Soc. 143 (2021) 14178–14188, https://doi.org/10.1021/jacs.1c04963;
(e) G.E. Sokolow, M.R. Crawley, D.R. Morphet, D. Asik, J.A. Spernyak, A.J. R. McGray, T.R. Cook, J.R. Morrow, Metal−organic polyhedron with four Fe(III) centers producing enhanced T1 magnetic resonance imaging contrast in tumors, Inorg. Chem. 61 (2022) 2603–2611, https://doi.org/10.1021/acs.inorgchem.1c03660.

[39] (a) R. Antwi-Baah, Y. Wang, X. Chen, K. Yu, Metal-based nanoparticle magnetic resonance imaging contrast agents: classifications, issues, and countermeasures toward their Clinical Translation, Adv. Mater. Interfaces 9 (2022), https://doi.org/10.1002/admi.202101710;
(b) G.J. Soufi, A. Hekmatnia, S. Iravani, R.S. Varma, Nanoscale contrast agents for magnetic resonance imaging: a review, ACS Appl. Nano Mater. 5 (2022) 10151–10166, https://doi.org/10.1021/acsanm.2c03297;
(c) S. Thangudu, E.-Y. Huang, C.-H. Su, Safe magnetic resonance imaging on biocompatible nanoformulations, Biomater. Sci. 10 (2022) 5032–5053, https://doi.org/10.1039/D2BM00692H;
(d) M. Liu, J. Yuan, G. Wang, N. Ni, Q. Lv, S. Liu, Y. Gong, X. Zhao, X. Wang, X. Sun, Shape programmable T1 – T2 dual-mode MRI nanoprobes for cancer theranostics, Nanoscale 15 (2023) 4694–4724, https://doi.org/10.1039/D2NR07009J;
(e) S.H. Lee, B.H. Kim, H. Bin Na, T. Hyeon, Paramagnetic inorganic nanoparticles as T1 MRI contrast agents, WIREs Nanomed. Nanobiotechnol. 6 (2014) 196–209, https://doi.org/10.1002/wnan.1243;
(f) X. Cai, Q. Zhu, Y. Zeng, Q. Zeng, X. Chen, Y. Zhan, Manganese oxide nanoparticles as MRI contrast agents in tumor multimodal imaging and therapy, Int. J. Nanomedicine 14 (2019) 8321–8344, https://doi.org/10.2147/IJN.S218085;
(g)F. Carniato, G. Gatti, ^{1}H NMR relaxometric analysis of paramagnetic Gd_2O_3:Yb nanoparticles functionalized with citrate groups, Inorganics 7 (2019) 34. doi:https://doi.org/10.3390/inorganics7030034;. (h) C. Chen, J. Ge, Y. Gao, L. Chen, J. Cui, J. Zeng, M. Gao, Ultrasmall superparamagnetic iron oxide nanoparticles: a next generation contrast agent for magnetic resonance imaging, WIREs Nanomed. Nanobiotechnol. 14 (2022), https://doi.org/10.1002/wnan.1740;
(i) F. Lux, V.L. Tran, E. Thomas, S. Dufort, F. Rossetti, M. Martini, C. Truillet, T. Doussineau, G. Bort, F. Denat, F. Boschetti, G. Angelovski, A. Detappe, Y. Crémillieux, N. Mignet, B.-T. Doan, B. Larrat, S. Meriaux, E. Barbier, S. Roux, P. Fries, A. Müller, M.-C. Abadjian, C. Anderson, E. Canet-Soulas, P. Bouziotis, M. Barberi-Heyob, C. Frochot, C. Verry, J. Balosso, M. Evans, J. Sidi-Boumedine, M. Janier, K. Butterworth, S. McMahon, K. Prise, M.-T. Aloy, D. Ardail, C. Rodriguez-Lafrasse, E. Porcel, S. Lacombe, R. Berbeco, A. Allouch, J.-L. Perfettini, C. Chargari, E. Deutsch, G. Le Duc, O. Tillement, AGuIX® from bench to bedside - Transfer of an ultrasmall theranostic gadolinium-based nanoparticle to clinical medicine, Br. J. Radiol. (2018) 20180365, https://doi.org/10.1259/bjr.20180365;
(j) F. Carniato, L. Tei, M. Botta, Gd-based mesoporous silica nanoparticles as MRI Probes, Eur. J. Inorg. Chem. 2018 (2018) 4936–4954, https://doi.org/10.1002/ejic.201801039;
(k) C.-T. Yang, P. Padmanabhan, B.Z. Gulyás, Gadolinium(III) based nanoparticles for T1-weighted magnetic resonance imaging probes, RSC Adv. 6 (2016) 60945–60966, https://doi.org/10.1039/C6RA07782J;
(l) V. Malytskyi, J. Moreau, M. Callewaert, G. Rigaux, C. Cadiou, S. Laurent, F. Chuburu, Organic nanoparticles and gadolinium chelates: seeking hypersensitive probes for T1 magnetic resonance imaging, Mater. Biomed. Eng., Elsevier (2019) 425–476, https://doi.org/10.1016/B978-0-12-818433-2.00013-3;
(m) C. Diaferia, E. Gianolo, A. Accardo, Peptide-based building blocks as structural elements for supramolecular Gd-containing MRI contrast agents, J. Pept. Sci. 25 (2019) e3157, https://doi.org/10.1002/psc.3157.

[40] X. Liu, J. Liu, S. Lin, X. Zhao, Hydrogel machines, Mater. Today 36 (2020) 102–124, https://doi.org/10.1016/j.mattod.2019.12.026.

[41] (a) T. Courant, V.G. Roullin, C. Cadiou, M. Callewaert, M.C. Andry, C. Portefaix, C. Hoeffel, M.C. de Goltstein, M. Port, S. Laurent, L. Vander Elst, R. Muller, M. Molinari, F. Chuburu, Hydrogels incorporating GdDOTA: towards highly efficient dual T1 /T2 MRI contrast agents, Angew. Chem. Int. Ed. 51 (2012) 9119–9122, https://doi.org/10.1002/anie.201203190;
(b) M. Callewaert, V.G. Roullin, C. Cadiou, E. Millart, L. Van Gulik, M.C. Andry, C. Portefaix, C. Hoeffel, S. Laurent, L. Vander Elst, R. Muller, M. Molinari, F. Chuburu, Tuning the composition of biocompatible Gd nanohydrogels to achieve hypersensitive dual T1 /T2 MRI contrast agents, J. Mater. Chem. B 2 (2014) 6397–6405, https://doi.org/10.1039/C4TB00783B;
(c) J. Moreau, M. Callewaert, V. Malytskyi, C. Henoumont, S.N. Voicu, M.S. Stan, M. Molinari, C. Cadiou, S. Laurent, F. Chuburu, Fluorescent chitosan-based nanohydrogels and encapsulation of gadolinium MRI contrast agent for magneto-optical imaging, Carbohydr. Polym. Technol. Appl. 2 (2021) 100104, https://doi.org/10.1016/j.carpta.2021.100104;
(d) G. Rigaux, C.V. Gheran, M. Callewaert, C. Cadiou, S.N. Voicu, A. Dinischiotu, M.C. Andry, L. Vander Elst, S. Laurent, R.N. Muller, A. Berquand, M. Molinari, S. Huclier-Markai, F. Chuburu, Characterization of Gd loaded chitosan-TPP nanohydrogels by a multi-technique approach combining dynamic light scattering (DLS), asymetrical flow-field-flow-fractionation (AF4) and atomic force microscopy (AFM) and design of positive contrast agents for molecular resonance imaging (MRI), Nanotechnology 28 (2017) 055705, https://doi.org/10.1088/1361-6528/aa5188;
(e) F. Carniato, M. Ricci, L. Tei, F. Garello, E. Terreno, E. Ravera, G. Parigi, C. Luchinat, M. Botta, High relaxivity with no coordinated waters: a seemingly paradoxical behavior of $[Gd(DOTP)]^{5-}$ embedded in nanogels, Inorg. Chem. 61 (2022) 5380–5387, https://doi.org/10.1021/acs.inorgchem.2c00225;
(f) F. Carniato, L. Tei, M. Botta, E. Ravera, M. Fragai, G. Parigi, C. Luchinat, ^{1}H NMR Relaxometric study of chitosan-based nanogels containing mono- and bis-hydrated Gd(III) chelates: clues for MRI probes of improved sensitivity, ACS Appl. Bio Mater. 3 (2020) 9065–9072, https://doi.org/10.1021/acsabm.0c01295;
(g) F. Carniato, M. Ricci, L. Tei, F. Garello, C. Furlan, E. Terreno, E. Ravera, G. Parigi, C. Luchinat, M. Botta, Novel nanogels loaded with Mn(II) chelates as effective and biologically stable MRI probes, Small 19 (2023), https://doi.org/10.1002/smll.202302868;
(h) M. Russo, A.M. Ponsiglione, E. Forte, P.A. Netti, E. Torino, Hydrodenticity to enhance relaxivity of gadolinium-DTPA within crosslinked hyaluronic acid nanoparticles, Nanomedicine 12 (2017) 2199–2210, https://doi.org/10.2217/nnm-2017-0098;
(i) F. De Sarno, A.M. Ponsiglione, M. Russo, A.M. Grimaldi, E. Forte, P.A. Netti, E. Torino, Water-mediated nanostructures for enhanced MRI: impact of water dynamics on relaxometric properties of Gd-DTPA, Theranostics 9 (2019) 1809–1824, https://doi.org/10.7150/thno.27313.

[42] E. Gallo, E. Rosa, C. Diaferia, F. Rossi, D. Tesauro, A. Accardo, Systematic overview of soft materials as a novel frontier for MRI contrast agents, RSC Adv. 10 (2020) 27064–27080, https://doi.org/10.1039/D0RA03194A.

[43] (a) T. Jones, D. Townsend, History and future technical innovation in positron emission tomography, J. Med. Imaging 4 (2017) 011013, https://doi.org/10.1117/1.JMI.4.1.011013;
(b) H. Herzog, *In vivo* functional imaging with SPECT and PET, Radiochim. Acta

89 (2001) 203–214, https://doi.org/10.1524/ract.2001.89.4-5.203;
(c) B.F. Hutton, The origins of SPECT and SPECT/CT, Eur. J. Nucl. Med. Mol. Imaging 41 (Suppl. 1) (2014) S3–S16, https://doi.org/10.1007/s00259-013-2606-5.

[44] (a) V. Kuntic, J. Brboric, Z. Vujic, S. Uskokovic-Markovic, Radioisotopes used as radiotracers for in vitro and in vivo diagnostics, Asian J. Chem. 28 (2016) 235–241, https://doi.org/10.14233/ajchem.2016.19401;
(b) G. Crișan, N.S. Moldovean-Cioroianu, D.-G. Timaru, G. Andrieș, C. Căinap, V. Chiș, Radiopharmaceuticals for PET and SPECT imaging: a literature review over the last decade, Int. J. Mol. Sci. 23 (2022) 5023, https://doi.org/10.3390/ijms23095023.

[45] A. Duatti, Review on ^{99m}Tc radiopharmaceuticals with emphasis on new advancements, Nucl. Med. Biol. 92 (2021) 202–216, https://doi.org/10.1016/j.nucmedbio.2020.05.005.

[46] (a) X. Deng, J. Rong, L. Wang, N. Vasdev, L. Zhang, L. Josephson, S.H. Liang, Chemistry for positron emission tomography: recent advances in ^{11}C-, ^{18}F-, ^{13}N-, and ^{15}O-labeling reactions, Angew. Chem. Int. Ed. 58 (2019) 2580–2605, https://doi.org/10.1002/anie.201805501;
(b) X. Zhong, J. Yan, X. Ding, C. Su, Y. Xu, M. Yang, Recent advances in bioorthogonal click chemistry for enhanced PET and SPECT Radiochemistry, Bioconjug. Chem. 34 (2023) 457–476, https://doi.org/10.1021/acs.bioconjchem.2c00583;
(c) L. Zhang, K. Hu, T. Shao, L. Hou, S. Zhang, W. Ye, L. Josephson, J.H. Meyer, M.-R. Zhang, N. Vasdev, J. Wang, H. Xu, L. Wang, S.H. Liang, Recent developments on PET radiotracers for TSPO and their applications in neuroimaging, Acta Pharm. Sin. B 11 (2021) 373–393, https://doi.org/10.1016/j.apsb.2020.08.006;
(d) A.T. Nguyen, H.-K. Kim, Recent developments in PET and SPECT radiotracers as radiopharmaceuticals for hypoxia tumors, Pharmaceutics 15 (2023) 1840, https://doi.org/10.3390/pharmaceutics15071840.

[47] (a) V. Liberini, R. Laudicella, M. Capozza, M.W. Huellner, I.A. Burger, S. Baldari, E. Terreno, D. Deandreis, The future of cancer diagnosis, treatment and sSurveillance: a systemic review on immunotherapy and immuno-PET radiotracers, Molecules 26 (2021) 2201, https://doi.org/10.3390/molecules26082201;
(b) M. Chomet, G.A.M.S. van Dongen, D.J. Vugts, State of the art in radiolabeling of antibodies with common and uncommon radiometals for preclinical and clinical immuno-PET, Bioconjug. Chem. 32 (2021) 1315–1330, https://doi.org/10.1021/acs.bioconjchem.1c00136;
(c) M. Farleigh, T.T. Pham, Z. Yu, J. Kim, K. Sunassee, G. Firth, N. Forte, V. Chudasama, J.R. Baker, N.J. Long, C. Rivas, M.T. Ma, New Bifunctional chelators incorporating dibromomaleimide groups for radiolabeling of antibodies with positron emission tomography imaging radioisotopes, Bioconjug. Chem. 32 (2021) 1214–1222, https://doi.org/10.1021/acs.bioconjchem.0c00710;
(d) M. Li, S. Wang, Q. Kong, X. Cheng, H. Yan, Y. Xing, X. Lan, D. Jiang, Advances in macrocyclic chelators for positron emission tomography imaging, VIEW 4 (2023), https://doi.org/10.1002/VIW.20230042.

[48] (a) E.W. Price, C. Orvig, Matching chelators to radiometals for radiopharmaceuticals, Chem. Soc. Rev. 43 (2014) 260–290, https://doi.org/10.1039/C3CS60304K;
(b) L. Lattuada, A. Barge, G. Cravotto, G.B. Giovenzana, L. Tei, The synthesis and application of polyamino polycarboxylic bifunctional chelating agents, Chem. Soc. Rev. 40 (2011) 3019, https://doi.org/10.1039/c0cs00199f.

[49] (a) A. Marlin, A. Koller, E. Madarasi, M. Cordier, D. Esteban-Gomez, C. Platas-Iglesias, G. Tircso, E. Boros, V. Patinec, R. Tripier, H_3NOTA derivatives possessing picolyl and picolinate pendants for Ga^{3+} coordination and $^{67}Ga^{3+}$ radiolabeling, Inorg. Chem. 62 (2023) 20634–20645, https://doi.org/10.1021/acs.inorgchem.3c01417;
(b) A. Marlin, I. Hierlmeier, A. Guillou, M. Bartholomä, R. Tripier, V. Patinec, Bioconjugated chelates based on (methylpyridinyl)TACN: synthesis, ^{64} Cu labeling and *in vitro* evaluation for prostate cancer targeting, Metallomics 14 (2022) mfac036, https://doi.org/10.1093/mtomcs/mfac036;
(c) A. Hu, J.J. Wilson, Advancing chelation strategies for large metal ions for nuclear medicine applications, Acc. Chem. Res. 55 (2022) 904–915, https://doi.org/10.1021/acs.accounts.2c00003;
(d) S.J. Raheem, B.W. Schmidt, V.R. Solomon, A.K. Salih, E.W. Price, Ultrasonic-assisted solid-phase peptide synthesis of DOTA-TATE and DOTA- linker -TATE derivatives as a simple and low-cost method for the facile synthesis of chelator–peptide conjugates, Bioconjug. Chem. 32 (2021) 1204–1213, https://doi.org/10.1021/acs.bioconjchem.0c00325;
(e) T. Grus, H. Lahnif, B. Klasen, E.-S. Moon, L. Greifenstein, F. Roesch, Squaric acid-based radiopharmaceuticals for tumor imaging and therapy, Bioconjug. Chem. 32 (2021) 1223–1231, https://doi.org/10.1021/acs.bioconjchem.1c00305;
(f) B.A. Vaughn, A.J. Koller, Z. Chen, S.H. Ahn, C.S. Loveless, S.J. Cingoranelli, Y. Yang, A. Cirri, C.J. Johnson, S.E. Lapi, K.W. Chapman, E. Boros, Homologous structural, chemical, and biological behavior of sc and lu complexes of the PICAGA bifunctional chelator: toward development of matched theranostic pairs for radiopharmaceutical applications, Bioconjug. Chem. 32 (2021) 1232–1241, https://doi.org/10.1021/acs.bioconjchem.0c00574;
(g) N. Herrero Álvarez, D. Bauer, J. Hernández-Gil, J.S. Lewis, Recent advances in radiometals for combined imaging and therapy in cancer, ChemMedChem 16 (2021) 2909–2941, https://doi.org/10.1002/cmdc.202100135;
(h) N. Choudhary, M. de Guadalupe Jaraquemada-Peláez, K. Zarschler, X. Wang, V. Radchenko, M. Kubeil, H. Stephan, C. Orvig, Chelation in one fell swoop: optimizing ligands for smaller radiometal ions, Inorg. Chem. 59 (2020) 5728–5741, https://doi.org/10.1021/acs.inorgchem.0c00509;
(i) Z. Baranyai, G. Tircsó, F. Rösch, The use of the macrocyclic chelator DOTA in radiochemical separations, Eur. J. Inorg. Chem. 2020 (2020) 36–56, https://doi.org/10.1002/ejic.201900706;
(j) E. Boros, J.P. Holland, Chemical aspects of metal ion chelation in the synthesis and application antibody-based radiotracers, J. Label. Compd. Radiopharm. 61 (2018) 652–671, https://doi.org/10.1002/jlcr.3590.

[50] (a) T.A. Lemaître, A.R. Burgoyne, M. Ooms, T.N. Parac-Vogt, T. Cardinaels, Inorganic radiolabeled nanomaterials in cancer therapy: a review, ACS Appl. Nano Mater. 5 (2022) 8680–8709, https://doi.org/10.1021/acsanm.2c01204;
(b) L. Aranda-Lara, B.E.O. García, K. Isaac-Olivé, G. Ferro-Flores, L. Meléndez-Alafort, E. Morales-Avila, Drug delivery systems-based dendrimers and polymer micelles for nuclear diagnosis and therapy, Macromol. Biosci. 21 (2021), https://doi.org/10.1002/mabi.202000362;
(c) S. Indoria, V. Singh, M.-F. Hsieh, Recent advances in theranostic polymeric nanoparticles for cancer treatment: a review, Int. J. Pharm. 582 (2020) 119314, https://doi.org/10.1016/j.ijpharm.2020.119314;
(d) L. Aranda-Lara, E. Morales-Avila, M.A. Luna-Gutiérrez, E. Olivé-Alvarez, K. Isaac-Olivé, Radiolabeled liposomes and lipoproteins as lipidic nanoparticles for imaging and therapy, Chem. Phys. Lipids 230 (2020) 104934, https://doi.org/10.1016/j.chemphyslip.2020.104934;
(e) D. Ni, E.B. Ehlerding, W. Cai, Multimodality imaging agents with PET as the fundamental pillar, Angew. Chem. Int. Ed. 58 (2019) 2570–2579, https://doi.org/10.1002/anie.201806853;
(f) F. Man, P.J. Gawne, R.T.M. de Rosales, Nuclear imaging of liposomal drug delivery systems: a critical review of radiolabelling methods and applications in nanomedicine, Adv. Drug Deliv. Rev. 143 (2019) 134–160, https://doi.org/10.1016/j.addr.2019.05.012.

[51] (a) M. Goel, Y. Mackeyev, S. Krishnan, Radiolabeled nanomaterial for cancer diagnostics and therapeutics: principles and concepts, Cancer Nanotechnol. 14 (2023) 15, https://doi.org/10.1186/s12645-023-00165-y;
(b) J. Pellico, P.J. Gawne, R.T.M. de Rosales, Radiolabelling of nanomaterials for medical imaging and therapy, Chem. Soc. Rev. 50 (2021) 3355–3423, https://doi.org/10.1039/D0CS00384K;
(c) J. Ge, Q. Zhang, J. Zeng, Z. Gu, M. Gao, Radiolabeling nanomaterials for multimodality imaging: new insights into nuclear medicine and cancer diagnosis, Biomaterials 228 (2020) 119553, https://doi.org/10.1016/j.biomaterials.2019.119553.

[52] (a) B.R. Masters, The development of fluorescence microscopy, in: Encyclopedia of Life Sciences (ELS), John Wiley & Sons, Ltd, Chichester, 2010, https://doi.org/10.1002/9780470015902.a0022093;
(b) M. Renz, Fluorescence microscopy - a historical and technical perspective, Cytometry Part A 83 (2013) 767–779, https://doi.org/10.1002/cyto.a.22295;
(c) B. Valeur, Introduction: on the origin of the terms fluorescence, phosphorescence, and luminescence, in: B. Valeur, J.C. Brochon (Eds.), New Trends in Fluorescence Spectroscopy. Springer Series on Fluorescence 1, Springer, Berlin, Heidelberg, 2001, https://doi.org/10.1007/978-3-642-56853-4_1.

[53] (a) B. Valeur, Molecular fluorescence, Wiley (2001), https://doi.org/10.1002/3527600248;
(b) J.R. Lakowicz (Ed.), Principles of fluorescence spectroscopy, Springer US, Boston, MA, 2006, https://doi.org/10.1007/978-0-387-46312-4.

[54] H. Kobayashi, M.R. Longmire, M. Ogawa, P.L. Choyke, Rational chemical design of the next generation of molecular imaging probes based on physics and biology: mixing modalities, colors and signals, Chem. Soc. Rev. 40 (2011) 4626, https://doi.org/10.1039/c1cs15077d.

[55] (a) C. Li, G. Chen, Y. Zhang, F. Wu, Q. Wang, Advanced fluorescence imaging technology in the near-infrared-II window for biomedical applications, J. Am. Chem. Soc. 142 (2020) 14789–14804, https://doi.org/10.1021/jacs.0c07022;
(b) P. Liu, X. Mu, X.-D. Zhang, D. Ming, The near-infrared-II fluorophores ana microscopy technologies development and application in bioimaging, Bioconjug. Chem. 31 (2020) 260–275, https://doi.org/10.1021/acs.bioconjchem.9b00610;
(c) S. Roy, N. Bag, S. Bardhan, I. Hasan, B. Guo, Recent progress in NIR-II fluorescence imaging-guided drug delivery for cancer theranostics, Adv. Drug Deliv. Rev. 197 (2023) 114821, https://doi.org/10.1016/j.addr.2023.114821.

[56] (a) G. Hong, A.L. Antaris, H. Dai, Near-infrared fluorophores for biomedical imaging, Nat. Biomed. Eng. 1 (2017) 0010, https://doi.org/10.1038/s41551-016-0010;
(b) S. Hameed, Z. Dai, Near-infrared fluorescence probes for surgical navigation, Mater. Today Chem. 10 (2018) 90–103, https://doi.org/10.1016/j.mtchem.2018.07.005;
(c) E.A. Owens, M. Henary, G. El Fakhri, H.S. Choi, Tissue-specific near-infrared fluorescence imaging, Acc. Chem. Res. 49 (2016) 1731–1740, https://doi.org/10.1021/acs.accounts.6b00239;
(d) X. Yi, F. Wang, W. Qin, X. Yang, J. Yuan, Near-infrared fluorescent probes in cancer imaging and therapy: an emerging field, Int. J. Nanomedicine (2014) 1347, https://doi.org/10.2147/IJN.S60206;
(e) L. Yuan, W. Lin, K. Zheng, L. He, W. Huang, Far-red to near-infrared analyte-responsive fluorescent probes based on organic fluorophore platforms for fluorescence imaging, Chem. Soc. Rev. 42 (2013) 622–661, https://doi.org/10.1039/C2CS35313J;
(f) S. Zeng, X. Liu, Y.S. Kafuti, H. Kim, J. Wang, X. Peng, H. Li, J. Yoon, Fluorescent dyes based on rhodamine derivatives for bioimaging and therapeutics: recent progress, challenges, and prospects, Chem. Soc. Rev. 52 (2023) 5607–5651, https://doi.org/10.1039/D2CS00799A;
(g) S. Lei, Y. Zhang, N.T. Blum, P. Huang, J. Lin, Recent advances in croconaine

dyes for bioimaging and theranostics, Bioconjug. Chem. 31 (2020) 2072–2084, https://doi.org/10.1021/acs.bioconjchem.0c00356.
[57] (a) D. Xue, D. Wu, Z. Lu, J. Neuhaus, A. Zebibula, Z. Feng, S. Cheng, J. Zhou, J. Qian, G. Li, Structural and functional NIR-II fluorescence bioimaging in urinary system via clinically approved dye methylene blue, Engineering 22 (2023) 149–158, https://doi.org/10.1016/j.eng.2021.07.032;
(b) L. Boni, G. David, A. Mangano, G. Dionigi, S. Rausei, S. Spampatti, E. Cassinotti, A. Fingerhut, Clinical applications of indocyanine green (ICG) enhanced fluorescence in laparoscopic surgery, Surg. Endosc. 29 (2015) 2046–2055, https://doi.org/10.1007/s00464-014-3895-x.
[58] Y. Ning, G.-Q. Jin, M.-X. Wang, S. Gao, J.-L. Zhang, Recent progress in metal-based molecular probes for optical bioimaging and biosensing, Curr. Opin. Chem. Biol. 66 (2022) 102097, https://doi.org/10.1016/j.cbpa.2021.102097.
[59] (a) Y. Ning, M. Zhu, J.-L. Zhang, Near-infrared (NIR) lanthanide molecular probes for bioimaging and biosensing, Coord. Chem. Rev. 399 (2019) 213028, https://doi.org/10.1016/j.ccr.2019.213028;
(b) J.-C.G. Bünzli, Lanthanide luminescence for biomedical analyses and imaging, Chem. Rev. 110 (2010) 2729–2755, https://doi.org/10.1021/cr900362e;
(c) H. Uh, S. Petoud, Novel antennae for the sensitization of near infrared luminescent lanthanide cations, Comptes Rendus. Chim. 13 (2010) 668–680, https://doi.org/10.1016/j.crci.2010.05.007.
[60] C. Zhu, L. Liu, Q. Yang, F. Lv, S. Wang, Water-soluble conjugated polymers for imaging, diagnosis, and therapy, Chem. Rev. 112 (2012) 4687–4735, https://doi.org/10.1021/cr200263w.
[61] (a) S. Pascal, S. David, C. Andraud, O. Maury, Near-infrared dyes for two-photon absorption in the short-wavelength infrared: strategies towards optical power limiting, Chem. Soc. Rev. 50 (2021) 6613–6658, https://doi.org/10.1039/D0CS01221A;
(b) P.A. Shaw, E. Forsyth, F. Haseeb, S. Yang, M. Bradley, M. Klausen, Two-photon absorption: an open door to the nir-ii biological window? Front. Chem. 10 (2022) https://doi.org/10.3389/fchem.2022.921354;
(c) K.H. Kim, S. Singha, Y.W. Jun, Y.J. Reo, H.R. Kim, H.G. Ryu, S. Bhunia, K. H. Ahn, Far-red/near-infrared emitting, two-photon absorbing, and bio-stable amino-Si-pyronin dyes, Chem. Sci. 10 (2019) 9028–9037, https://doi.org/10.1039/C9SC02287B;
(d) N. Hamon, A. Roux, M. Beyler, J.-C. Mulatier, C. Andraud, C. Nguyen, M. Maynadier, N. Bettache, A. Duperray, A. Grichine, s. brasselet, m. gary-bobo, o. maury, r., tripier, pyclen-based ln(iii) complexes as highly luminescent bioprobes for in vitro and in vivo one- and two-photon bioimaging Applications, J. Am. Chem. Soc. 142 (2020) 10184–10197, https://doi.org/10.1021/jacs.0c03496;
(e) M.Y. Berezin, C. Zhan, H. Lee, C. Joo, W.J. Akers, S. Yazdanfar, S. Achilefu, Two-photon optical properties of near-infrared dyes at 1.55 μm excitation, J. Phys. Chem. B 115 (2011) 11530–11535, https://doi.org/10.1021/jp207618e.
[62] (a) Z. Wang, Y. Zhou, R. Xu, Y. Xu, D. Dang, Q. Shen, L. Meng, B.Z. Tang, Seeing the unseen: aie luminogens for super-resolution imaging, Coord. Chem. Rev. 451 (2022) 214279, https://doi.org/10.1016/j.ccr.2021.214279;
(b) S. Liu, Y. Li, R.T.K. Kwok, J.W.Y. Lam, B.Z. Tang, Structural and process controls of AIEgens for NIR-II theranostics, Chem. Sci. 12 (2021) 3427–3436, https://doi.org/10.1039/D0SC02911D;
(c) H. Li, H. Kim, J. Han, V. Nguyen, X. Peng, J. Yoon, Activity-based smart AIEgens for detection, bioimaging, and therapeutics: recent progress and outlook, Aggregate 2 (2021) e51, https://doi.org/10.1002/agt2.51;
(d) Y. Wang, Y. Zhang, J. Wang, X.-J. Liang, Aggregation-induced emission (AIE) fluorophores as imaging tools to trace the biological fate of nano-based drug delivery systems, Adv. Drug Deliv. Rev. 143 (2019) 161–176, https://doi.org/10.1016/j.addr.2018.12.004;
(e) J. Li, Z. Feng, X. Yu, D. Wu, T. Wu, J. Qian, Aggregation-induced emission fluorophores towards the second near-infrared optical windows with suppressed imaging background, Coord. Chem. Rev. 472 (2022) 214792, https://doi.org/10.1016/j.ccr.2022.214792;
(f) Y. Li, Z. Cai, S. Liu, H. Zhang, S.T.H. Wong, J.W.Y. Lam, R.T.K. Kwok, J. Qian, B.Z. Tang, Design of AIEgens for near-infrared IIb imaging through structural modulation at molecular and morphological levels, Nat. Commun. 11 (2020) 1255, https://doi.org/10.1038/s41467-020-15095-1.
[63] (a) W. Li, G.S. Kaminski Schierle, B. Lei, Y. Liu, C.F. Kaminski, Fluorescent nanoparticles for super-resolution imaging, Chem. Rev. 122 (2022) 12495–12543, https://doi.org/10.1021/acs.chemrev.2c00050;
(b) L. Zhang, Y. Liu, H. Huang, H. Xie, B. Zhang, W. Xia, B. Guo, Multifunctional nanotheranostics for near infrared optical imaging-guided treatment of brain tumors, Adv. Drug Deliv. Rev. 190 (2022) 114536, https://doi.org/10.1016/j.addr.2022.114536;
(c) F. Yang, Q. Zhang, S. Huang, D. Ma, Recent advances of near infrared inorganic fluorescent probes for biomedical applications, J. Mater. Chem. B 8 (2020) 7856–7879, https://doi.org/10.1039/D0TB01430C;
(d) Y. Cai, Z. Wei, C. Song, C. Tang, W. Han, X. Dong, Optical nano-agents in the second near-infrared window for biomedical applications, Chem. Soc. Rev. 48 (2019) 22–37, https://doi.org/10.1039/C8CS00494C;
(e) Y. Kenry, B. Duan, Liu, Recent advances of optical imaging in the second near-infrared window, Adv. Mater. 30 (2018), https://doi.org/10.1002/adma.201802394;
(f) I. Martinić, S.V. Eliseeva, S. Petoud, Near-infrared emitting probes for biological imaging: organic fluorophores, quantum dots, fluorescent proteins, lanthanide(III) complexes and nanomaterials, J. Lumin. 189 (2017) 19–43, https://doi.org/10.1016/j.jlumin.2016.09.058.
[64] (a) S. Pandey, D. Bodas, High-quality quantum dots for multiplexed bioimaging: a critical review, Adv. Colloid Interf. Sci. 278 (2020) 102137, https://doi.org/10.1016/j.cis.2020.102137;
(b) B. Gidwani, V. Sahu, S.S. Shukla, R. Pandey, V. Joshi, V.K. Jain, A. Vyas, Quantum dots: prospectives, toxicity, advances and applications, J. Drug Deliv. Sci. Technol. 61 (2021) 102308, https://doi.org/10.1016/j.jddst.2020.102308.
[65] (a) Y. Xu, W. Yang, D. Yao, K. Bian, W. Zeng, K. Liu, D. Wang, B. Zhang, An aggregation-induced emission dye-powered afterglow luminogen for tumor imaging, Chem. Sci. 11 (2020) 419–428, https://doi.org/10.1039/C9SC04901K;
(b) J. Li, K. Pu, Development of organic semiconducting materials for deep-tissue optical imaging, phototherapy and photoactivation, Chem. Soc. Rev. 48 (2019) 38–71, https://doi.org/10.1039/C8CS00001H;
(c) J. Lin, X. Zeng, Y. Xiao, L. Tang, J. Nong, Y. Liu, H. Zhou, B. Ding, F. Xu, H. Tong, Z. Deng, X. Hong, Novel near-infrared II aggregation-induced emission dots for in vivo bioimaging, Chem. Sci. 10 (2019) 1219–1226, https://doi.org/10.1039/C8SC04363A.
[66] (a) N. Panwar, A.M. Soehartono, K.K. Chan, S. Zeng, G. Xu, J. Qu, P. Coquet, K.-T. Yong, X. Chen, nanocarbons for biology and medicine: sensing, imaging, and drug delivery, Chem. Rev. 119 (2019) 9559–9656, https://doi.org/10.1021/acs.chemrev.9b00099;
(b) E.M. Hofferber, J.A. Stapleton, N.M. Iverson, Review - single walled carbon nanotubes as optical sensors for biological applications, J. Electrochem. Soc. 167 (2020) 037530, https://doi.org/10.1149/1945-7111/ab64bf;
(c) T. Takeuchi, Y. Iizumi, M. Yudasaka, S. Kizaka-Kondoh, T. Okazaki, Characterization and biodistribution analysis of oxygen-doped single-walled carbon nanotubes used as in vivo fluorescence imaging probes, Bioconjug. Chem. 30 (2019) 1323–1330, https://doi.org/10.1021/acs.bioconjchem.9b00088;
(d) A.K. Mandal, X. Wu, J.S. Ferreira, M. Kim, L.R. Powell, H. Kwon, L. Groc, Y. Wang, L. Cognet, Fluorescent sp^3 defect-tailored carbon nanotubes enable NIR-II single particle imaging in live brain slices at ultra-low excitation doses, Sci. Rep. 10 (2020) 5286, https://doi.org/10.1038/s41598-020-62201-w;
(e) X. Li, S. Zhao, B. Li, K. Yang, M. Lan, L. Zeng, Advances and perspectives in carbon dot-based fluorescent probes: mechanism, and application, Coord. Chem. Rev. 431 (2021) 213686, https://doi.org/10.1016/j.ccr.2020.213686;
(f) Y. Li, G. Bai, S. Zeng, J. Hao, Theranostic carbon dots with innovative NIR-II emission for in vivo renal-excreted optical imaging and photothermal therapy, ACS Appl. Mater. Interfaces 11 (2019) 4737–4744, https://doi.org/10.1021/acsami.8b14877;
(g) M.O. Alas, F.B. Alkas, A. Aktas Sukuroglu, R. Genc Alturk, D. Battal, Fluorescent carbon dots are the new quantum dots: an overview of their potential in emerging technologies and nanosafety, J. Mater. Sci. 55 (2020) 15074–15105, https://doi.org/10.1007/s10853-020-05054-y.
[67] (a) Y. Wu, M.R.K. Ali, K. Chen, N. Fang, M.A. El-Sayed, Gold nanoparticles in biological optical imaging, Nano Today 24 (2019) 120–140, https://doi.org/10.1016/j.nantod.2018.12.006;
(b) C. de la Encarnación, D. Jimenez de Aberasturi, L.M. Liz-Marzán, Multifunctional plasmonic-magnetic nanoparticles for bioimaging and hyperthermia, Adv. Drug Deliv. Rev. 189 (2022) 114484, https://doi.org/10.1016/j.addr.2022.114484;
(c) P. Si, N. Razmi, O. Nur, S. Solanki, C.M. Pandey, R.K. Gupta, B.D. Malhotra, M. Willander, A. de la Zerda, Gold nanomaterials for optical biosensing and bioimaging, Nanoscale Adv. 3 (2021) 2679–2698, https://doi.org/10.1039/D0NA00961J;
(d) R. Kotcherlakota, S. Nimushakavi, A. Roy, H.C. Yadavalli, S. Mukherjee, S. Haque, C.R. Patra, Biosynthesized gold nanoparticles: in vivo study of near-infrared fluorescence (NIR)-based bio-imaging and cell labeling applications, ACS Biomater. Sci. Eng. 5 (2019) 5439–5452, https://doi.org/10.1021/acsbiomaterials.9b00721;
(e) A. Sani, C. Cao, D. Cui, Toxicity of gold nanoparticles (AuNPs): a review, Biochem. Biophys. Rep. 26 (2021) 100991, https://doi.org/10.1016/j.bbrep.2021.100991.
[68] (a) M. Haase, H. Schäfer, Upconverting Nanoparticles, Angew. Chem. Int. Ed. 50 (2011) 5808–5829, https://doi.org/10.1002/anie.201005159;
(b) Y. Zhang, X. Zhu, Y. Zhang, Exploring heterostructured upconversion nanoparticles: from rational engineering to diverse applications, ACS Nano 15 (2021) 3709–3735, https://doi.org/10.1021/acsnano.0c09231;
(c) C. Yan, H. Zhao, D.F. Perepichka, F. Rosei, Lanthanide ion doped upconverting nanoparticles: synthesis, structure and properties, Small 12 (2016) 3888–3907, https://doi.org/10.1002/smll.201601565;
(d)L.J. Charbonnière, Bringing upconversion down to the molecular scale, Dalton Trans. 47 (2018) 8566–8570. doi:10.1039/C7DT04737A. (e) A. Nonat, C. F. Chan, T. Liu, C. Platas-Iglesias, Z. Liu, W.-T. Wong, W.-K. Wong, K.-L. Wong, L. J. Charbonnière, Room temperature molecular upconversion in solution, Nat. Commun. 7 (2016) 11978, https://doi.org/10.1038/ncomms11978;
(f) A. Nonat, S. Bahamyirou, A. Lecointre, F. Przybilla, Y. Mély, C. Platas-Iglesias, F. Camerel, O. Jeannin, L.J. Charbonnière, Molecular upconversion in water in heteropolynuclear supramolecular Tb/Yb assemblies, J. Am. Chem. Soc. 141 (2019) 1568–1576, https://doi.org/10.1021/jacs.8b10932;
(g) A.M. Nonat, L.J. Charbonnière, Upconversion of light with molecular and supramolecular lanthanide complexes, Coord. Chem. Rev. 409 (2020) 213192, https://doi.org/10.1016/j.ccr.2020.213192;
(h) Q. Ma, J. Wang, Z. Li, X. Lv, L. Liang, Q. Yuan, Recent progress in time-resolved biosensing and bioimaging based on lanthanide-doped nanoparticles, Small 15 (2019), https://doi.org/10.1002/smll.201804969;
(i) M. Matulionyte, A. Skripka, A. Ramos-Guerra, A. Benayas, F. Vetrone, The coming of age of neodymium: redefining its role in rare earth doped

nanoparticles, Chem. Rev. 123 (2023) 515–554, https://doi.org/10.1021/acs.chemrev.2c00419;
(j) Y. Zhong, Z. Ma, F. Wang, X. Wang, Y. Yang, Y. Liu, X. Zhao, J. Li, H. Du, M. Zhang, Q. Cui, S. Zhu, Q. Sun, H. Wan, Y. Tian, Q. Liu, W. Wang, K.C. Garcia, H. Dai, In vivo molecular imaging for immunotherapy using ultra-bright near-infrared-IIb rare-earth nanoparticles, Nat. Biotechnol. 37 (2019) 1322–1331, https://doi.org/10.1038/s41587-019-0262-4;
(k) Y. Fan, F. Zhang, A new generation of NIR-II probes: lanthanide-based nanocrystals for bioimaging and biosensing, Adv. Opt. Mater. 7 (2019), https://doi.org/10.1002/adom.201801417;
(l) A. Gnach, T. Lipinski, A. Bednarkiewicz, J. Rybka, J.A. Capobianco, Upconverting nanoparticles: assessing the toxicity, Chem. Soc. Rev. 44 (2015) 1561–1584, https://doi.org/10.1039/C4CS00177J.

[69] (a) A.G. Bell, On the production and reproduction of sound by light, Am. J. Sci. s3-20 (1880) 305–324, https://doi.org/10.2475/ajs.s3-20.118.305;
(b) J. Tyndall, Action of an intermittent beam of radiant heat upon gaseous matter, Proc. R. Soc. Lond. 31 (1881) 307–317, https://doi.org/10.1098/rspl.1880.0037;
(c) W.C. Röntgen, Ueber Töne, welche durch intermittirende Bestrahlung eines Gases entstehen, Ann. Phys. 248 (1881) 155–159, https://doi.org/10.1002/andp.18812480114;
(d) S. Manohar, D. Razansky, Photoacoustics: a historical review, Adv. Opt. Photon. 8 (2016) 586, https://doi.org/10.1364/AOP.8.000586.

[70] J. Yao, L.V. Wang, Photoacoustic tomography: fundamentals, advances and prospects, Contrast Media Mol. Imaging 6 (2011) 332–345, https://doi.org/10.1002/cmmi.443.

[71] R.A. Kruger, R.B. Lam, D.R. Reinecke, S.P. Del Rio, R.P. Doyle, Photoacoustic angiography of the breast, Med. Phys. 37 (2010) 6096–6100, https://doi.org/10.1118/1.3497677.

[72] K. Homan, S. Kim, Y.-S. Chen, B. Wang, S. Mallidi, S. Emelianov, Prospects of molecular photoacoustic imaging at 1064 nm wavelength, Opt. Lett. 35 (2010) 2663, https://doi.org/10.1364/OL.35.002663.

[73] P. Beard, Biomedical photoacoustic imaging, Interface Focus 1 (2011) 602–631, https://doi.org/10.1098/rsfs.2011.0028.

[74] D. Finch, S.K. Patch, Determining a function from its mean values over a family of spheres, SIAM J. Math. Anal. 35 (2004) 1213–1240, https://doi.org/10.1137/S0036141002417814.

[75] L.A. Kunyansky, Explicit inversion formulae for the spherical mean radon transform, Inverse Probl. 23 (2007) 373–383, https://doi.org/10.1088/0266-5611/23/1/021.

[76] M. Xu, L.V. Wang, Universal back-projection algorithm for photoacoustic computed tomography, Phys. Rev. E 71 (2005) 016706, https://doi.org/10.1103/PhysRevE.71.016706.

[77] J. Xia, L.V. Wang, Small-animal whole-body photoacoustic tomography: a review, IEEE Trans. Biomed. Eng. 61 (2014) 1380–1389, https://doi.org/10.1109/TBME.2013.2283507.

[78] L.V. Wang, L. Gao, Photoacoustic microscopy and computed tomography: from bench to bedside, Annu. Rev. Biomed. Eng. 16 (2014) 155–185, https://doi.org/10.1146/annurev-bioeng-071813-104553.

[79] (a) V. Ntziachristos, D. Razansky, Molecular imaging by means of multispectral optoacoustic tomography (MSOT), Chem. Rev. 110 (2010) 2783–2794, https://doi.org/10.1021/cr9002566;
(b) L. Nie, X. Chen, Structural and functional photoacoustic molecular tomography aided by emerging contrast agents, Chem. Soc. Rev. 43 (2014) 7132–7170, https://doi.org/10.1039/C4CS00086B;
(c) X.L. Deán-Ben, S. Gottschalk, B. Mc Larney, S. Shoham, D. Razansky, Advanced optoacoustic methods for multiscale imaging of in vivo dynamics, Chem. Soc. Rev. 46 (2017) 2158–2198, https://doi.org/10.1039/C6CS00765A;
(d) D. Razansky, J. Klohs, R. Ni, Multi-scale optoacoustic molecular imaging of brain diseases, Eur. J. Nucl. Med. Mol. Imaging 48 (2021) 4152–4170, https://doi.org/10.1007/s00259-021-05207-4;
(e) X. Hui, M.O.A. Malik, M. Pramanik, Looking deep inside tissue with photoacoustic molecular probes: a review, J. Biomed. Opt. 27 (2022), https://doi.org/10.1117/1.JBO.27.7.070901.

[80] S. Hu, L.V. Wang, Optical-resolution photoacoustic microscopy: auscultation of biological systems at the cellular level, Biophys. J. 105 (2013) 841–847, https://doi.org/10.1016/j.bpj.2013.07.017.

[81] Y. Zhou, G. Li, L. Zhu, C. Li, L.A. Cornelius, L.V. Wang, Handheld photoacoustic probe to detect both melanoma depth and volume at high speed in vivo, J. Biophotonics 8 (2015) 961–967, https://doi.org/10.1002/jbio.201400143.

[82] Z. Xu, C. Li, L.V. Wang, Photoacoustic tomography of water in phantoms and tissue, J. Biomed. Opt. 15 (2010) 036019, https://doi.org/10.1117/1.3443793.

[83] T. Wang, M.N. Ma, S. Slipchenko, J. Liang, K.K. Hui, S. Shung, M. Roy, Q. Sturek, Z. Zhou, J.-X. Chen, Cheng, High-speed intravascular photoacoustic imaging of lipid-laden atherosclerotic plaque enabled by a 2-kHz barium nitrite Raman laser, Sci. Rep. 4 (2014) 6889, https://doi.org/10.1038/srep06889.

[84] (a) N. Liu, K. Mishra, A.C. Stiel, V. Gujrati, V. Ntziachristos, The sound of drug delivery: optoacoustic imaging in pharmacology, Adv. Drug Deliv. Rev. 189 (2022) 114506, https://doi.org/10.1016/j.addr.2022.114506;
(b) P.K. Upputuri, M. Pramanik, Recent advances in photoacoustic contrast agents for in vivo imaging, WIREs Nanomed. Nanobiotechnol. 12 (2020), https://doi.org/10.1002/wnan.1618;
(c) Q. Fu, R. Zhu, J. Song, H. Yang, X. Chen, Photoacoustic imaging: contrast agents and their biomedical applications, Adv. Mater. 31 (2019), https://doi.org/10.1002/adma.201805875.

[85] (a) Y. Mantri, J.V. Jokerst, Engineering plasmonic nanoparticles for enhanced photoacoustic imaging, ACS Nano 14 (2020) 9408–9422, https://doi.org/10.1021/acsnano.0c05215;
(b) W. Li, X. Chen, Gold nanoparticles for photoacoustic imaging, Nanomedicine 10 (2015) 299–320, https://doi.org/10.2217/nnm.14.169;
(c) J. Zhong, L. Wen, S. Yang, L. Xiang, Q. Chen, D. Xing, Imaging-guided high-efficient photoacoustic tumor therapy with targeting gold nanorods, Nanomedicine Nanotechnology, Biol. Med. 11 (2015) 1499–1509, https://doi.org/10.1016/j.nano.2015.04.002;
(d) S. Wang, Z. Teng, P. Huang, D. Liu, Y. Liu, Y. Tian, J. Sun, Y. Li, H. Ju, X. Chen, G. Lu, Reversibly extracellular pH controlled cellular uptake and photothermal therapy by PEGylated mixed-charge gold nanostars, Small 11 (2015) 1801–1810, https://doi.org/10.1002/smll.201403248;
(e) T. Sun, Y. Wang, Y. Wang, J. Xu, X. Zhao, S. Vangveravong, R.H. Mach, Y. Xia, Using SV119-Gold Nanocage conjugates to eradicate cancer stem cells through a combination of photothermal and chemo therapies, Adv. Healthc. Mater. 3 (2014) 1283–1291, https://doi.org/10.1002/adhm.201400026;
(f) J. Song, X. Yang, O. Jacobson, P. Huang, X. Sun, L. Lin, X. Yan, G. Niu, Q. Ma, X. Chen, Ultrasmall gold nanorod vesicles with enhanced tumor accumulation and fast excretion from the body for cancer therapy, Adv. Mater. 27 (2015) 4910–4917, https://doi.org/10.1002/adma.201502486;
(g) X. Cheng, X. Zhou, J. Xu, R. Sun, H. Xia, J. Ding, Y.E. Chin, Z. Chai, H. Shi, M. Gao, Furin enzyme and ph synergistically triggered aggregation of gold nanoparticles for activated photoacoustic imaging and photothermal therapy of tumors, Anal. Chem. 93 (2021) 9277–9285, https://doi.org/10.1021/acs.analchem.1c01713;
(h) A. Balfourier, N. Luciani, G. Wang, G. Lelong, O. Ersen, A. Khelfa, D. Alloyeau, F. Gazeau, F. Carn, Unexpected intracellular biodegradation and recrystallization of gold nanoparticles, Proc. Natl. Acad. Sci. 117 (2020) 103–113, https://doi.org/10.1073/pnas.1911734116.

[86] S.K. Maji, S. Sreejith, J. Joseph, M. Lin, T. He, Y. Tong, H. Sun, S.W. Yu, Y. Zhao, Upconversion nanoparticles as a contrast agent for photoacoustic imaging in live mice, Adv. Mater. 26 (2014) 5633–5638, https://doi.org/10.1002/adma.201400831.

[87] (a) S. Jeong, S.W. Yoo, H.J. Kim, J. Park, J.W. Kim, C. Lee, H. Kim, Recent progress on molecular photoacoustic imaging with carbon-based nanocomposites, Materials (Basel) 14 (2021) 5643, https://doi.org/10.3390/ma14195643;
(b) L. Zhang, P. Rong, M. Chen, S. Gao, L. Zhu, A novel single walled carbon nanotube (SWCNT) functionalization agent facilitating in vivo combined chemo/thermo therapy, Nanoscale 7 (2015) 16204–16213, https://doi.org/10.1039/C5NR03752B;
(c) J. Lin, X. Chen, P. Huang, Graphene-based nanomaterials for bioimaging, Adv. Drug Deliv. Rev. 105 (2016) 242–254, https://doi.org/10.1016/j.addr.2016.05.013;
(d) J. Ge, Q. Jia, W. Liu, L. Guo, Q. Liu, M. Lan, H. Zhang, X. Meng, P. Wang, Red-emissive carbon dots for fluorescent, photoacoustic, and thermal theranostics in living mice, Adv. Mater. 27 (2015) 4169–4177, https://doi.org/10.1002/adma.201500323;
(e) Z. Jia, R. Dai, Z. Zheng, Y. Qin, A. Duan, X. Peng, X. Xie, R. Zhang, Hollow carbon-based nanosystem for photoacoustic imaging-guided hydrogenothermal therapy in the second near-infrared window, RSC Adv. 11 (2021) 12022–12029, https://doi.org/10.1039/D1RA00093D;
(f) R. Madannejad, N. Shoaie, F. Jahanpeyma, M.H. Darvishi, M. Azimzadeh, H. Javadi, Toxicity of carbon-based nanomaterials: reviewing recent reports in medical and biological systems, Chem. Biol. Interact. 307 (2019) 206–222, https://doi.org/10.1016/j.cbi.2019.04.036.

[88] (a) J. Wu, T. Hu, G. Zhao, A. Li, R. Liang, Two-dimensional transition metal chalcogenide nanomaterials for cancer diagnosis and treatment, Chin. Chem. Lett. 33 (2022) 4437–4448, https://doi.org/10.1016/j.cclet.2021.12.080;
(b) X. Zhou, H. Sun, X. Bai, Two-dimensional transition metal dichalcogenides: synthesis, biomedical applications and biosafety evaluation, Front. Bioeng. Biotechnol. 8 (2020), https://doi.org/10.3389/fbioe.2020.00236;
(c) C.M. Hessel, V.P. Pattani, M. Rasch, M.G. Panthani, B. Koo, J.W. Tunnell, B. A. Korgel, Copper selenide nanocrystals for photothermal therapy, Nano Lett. 11 (2011) 2560–2566, https://doi.org/10.1021/nl201400z;
(d) L. Cheng, J. Liu, X. Gu, H. Gong, X. Shi, T. Liu, C. Wang, X. Wang, G. Liu, H. Xing, W. Bu, B. Sun, Z. Liu, PEGylated WS_2 nanosheets as a multifunctional theranostic agent for in vivo dual-modal ct/photoacoustic imaging guided photothermal therapy, Adv. Mater. 26 (2014) 1886–1893, https://doi.org/10.1002/adma.201304497;
(e) W. Yin, L. Yan, J. Yu, G. Tian, L. Zhou, X. Zheng, X. Zhang, Y. Yong, J. Li, Z. Gu, Y. Zhao, High-throughput synthesis of single-layer MoS_2 nanosheets as a near-infrared photothermal-triggered drug delivery for effective cancer therapy, ACS Nano 8 (2014) 6922–6933, https://doi.org/10.1021/nn501647j.

[89] (a) M. Luo, T. Fan, Y. Zhou, H. Zhang, L. Mei, 2D Black phosphorus–based biomedical applications, Adv. Funct. Mater. 29 (2019), https://doi.org/10.1002/adfm.201808306;
(b) X. Qian, Z. Gu, Y. Chen, Two-dimensional black phosphorus nanosheets for theranostic nanomedicine, Mater. Horizons 4 (2017) 800–816, https://doi.org/10.1039/C7MH00305F;
(c) C. Sun, L. Wen, J. Zeng, Y. Wang, Q. Sun, L. Deng, C. Zhao, Z. Li, One-pot solventless preparation of PEGylated black phosphorus nanoparticles for photoacoustic imaging and photothermal therapy of cancer, Biomaterials 91 (2016) 81–89, https://doi.org/10.1016/j.biomaterials.2016.03.022;
(d) H. Wang, X. Yang, W. Shao, S. Chen, J. Xie, X. Zhang, J. Wang, Y. Xie, Ultrathin black phosphorus nanosheets for efficient singlet oxygen generation,

J. Am. Chem. Soc. 137 (2015) 11376–11382, https://doi.org/10.1021/jacs.5b06025;
(e) X. Zhang, I.S. Donskyi, W. Tang, S. Deng, D. Liu, S. Zhang, Q. Zhao, B. Xing, Biological effects of black phosphorus nanomaterials on mammalian cells and animals, Angew. Chem. Int. Ed. 62 (2023), https://doi.org/10.1002/anie.202213336.

[90] (a) Y. Qiu, B. Yuan, Y. Cao, X. He, O.U. Akakuru, L. Lu, N. Chen, M. Xu, A. Wu, J. Li, Recent progress on near-infrared fluorescence heptamethine cyanine dye-based molecules and nanoparticles for tumor imaging and treatment, WIREs Nanomed. Nanobiotechnol. 15 (2023), https://doi.org/10.1002/wnan.1910;
(b) A. St, E.R. Lorenz, O. Buabeng, O. Taratula, M. Henary Taratula, Near-infrared heptamethine cyanine dyes for nanoparticle-based photoacoustic imaging and photothermal therapy, J. Med. Chem. 64 (2021) 8798–8805, https://doi.org/10.1021/acs.jmedchem.1c00771;
(c) L. Feng, W. Chen, X. Ma, S.H. Liu, J. Yin, Near-infrared heptamethine cyanines (Cy7): from structure, property to application, Org. Biomol. Chem. 18 (2020) 9385–9397, https://doi.org/10.1039/D0OB01962C;
(d) C. Sun, W. Du, B. Wang, B. Dong, B. Wang, Research progress of near-infrared fluorescence probes based on indole heptamethine cyanine dyes in vivo and in vitro, BMC Chem. 14 (2020) 21, https://doi.org/10.1186/s13065-020-00677-3;
(e) A. Mishra, Y. Jiang, S. Roberts, V. Ntziachristos, G.G. Westmeyer, Near-infrared photoacoustic imaging probe responsive to calcium, Anal. Chem. 88 (2016) 10785–10789, https://doi.org/10.1021/acs.analchem.6b03039;
(f) A. Mishra, R.K. Behera, P.K. Behera, B.K. Mishra, G.B. Behera, Cyanines during the 1990s: a review, Chem. Rev. 100 (2000) 1973–2012, https://doi.org/10.1021/cr990402t.

[91] (a) G. Kim, S.-W. Huang, K.C. Day, M. O'Donnell, R.R. Agayan, M.A. Day, R. Kopelman, S. Ashkenazi, Indocyanine-green-embedded PEBBLEs as a contrast agent for photoacoustic imaging, J. Biomed. Opt. 12 (2007) 044020, https://doi.org/10.1117/1.2771530;
(b)K.M. Stantz, M. Cao, B. Liu, K.D. Miller, L. Guo, Molecular imaging of neutropilin-1 receptor using photoacoustic spectroscopy in breast tumors, in: A.A. Oraevsky, L. V. Wang (Eds.), 2010: p. 75641O. doi:10.1117/12.842271;. (c) S. Bhattacharyya, S. Wang, D. Reinecke, W. Kiser, R.A. Kruger, T.R. DeGrado, Synthesis and evaluation of near-infrared (NIR) dye−herceptin conjugates as photoacoustic computed tomography (PCT) probes for HER2 expression in breast cancer, Bioconjug. Chem. 19 (2008) 1186–1193, https://doi.org/10.1021/bc700482u.

[92] (a) H.S. Choi, K. Nasr, S. Alyabyev, D. Feith, J.H. Lee, S.H. Kim, Y. Ashitate, H. Hyun, G. Patonay, L. Strekowski, M. Henary, J.V. Frangioni, Synthesis and in vivo fate of zwitterionic near-infrared fluorophores, Angew. Chem. Int. Ed. 50 (2011) 6258–6263, https://doi.org/10.1002/anie.201102459;
(b) H. Hyun, M.W. Bordo, K. Nasr, D. Feith, J.H. Lee, S.H. Kim, Y. Ashitate, L. A. Moffitt, M. Rosenberg, M. Henary, H.S. Choi, J.V. Frangioni, cGMP-Compatible preparative scale synthesis of near-infrared fluorophores, Contrast Media Mol. Imaging 7 (2012) 516–524, https://doi.org/10.1002/cmmi.1484;
(c) D. Su, C.L. Teoh, S.-J. Park, J.-J. Kim, A. Samanta, R. Bi, U.S. Dinish, M. Olivo, M. Piantino, F. Louis, M. Matsusaki, S.S. Kim, M.A. Bae, Y.-T. Chang, Seeing elastin: a Near-infrared zwitterionic fluorescent probe for in vivo elastin imaging, Chem 4 (2018) 1128–1138, https://doi.org/10.1016/j.chempr.2018.02.016;
(d) S.H. Kim, J.H. Lee, H. Hyun, Y. Ashitate, G. Park, K. Robichaud, E. Lunsford, S.J. Lee, G. Khang, H.S. Choi, Near-infrared fluorescence imaging for noninvasive trafficking of scaffold degradation, Sci. Rep. 3 (2013) 1198, https://doi.org/10.1038/srep01198.

[93] (a) U. Chitgupi, N. Nyayapathi, J. Kim, D. Wang, B. Sun, C. Li, K. Carter, W. Huang, C. Kim, J. Xia, J.F. Lovell, Surfactant-stripped micelles for NIR-II photoacoustic imaging through 12 cm of breast tissue and whole human breasts, Adv. Mater. 31 (2019), https://doi.org/10.1002/adma.201902279;
(b) W. Zhou, L. Yin, X. Zhang, T. Liang, Z. Guo, Y. Liu, C. Xie, Q. Fan, Recent advances in small molecule dye-based nanotheranostics for NIR-II photoacoustic imaging-guided cancer therapy, Front. Bioeng. Biotechnol. 10 (2022), https://doi.org/10.3389/fbioe.2022.1002006;
(c) C. Song, Y. Li, T. Li, Y. Yang, Z. Huang, J.M. de la Fuente, J. Ni, D. Cui, Long-circulating drug-dye-based micelles with ultrahigh pH-sensitivity for deep tumor penetration and superior chemo-photothermal therapy, Adv. Funct. Mater. 30 (2020), https://doi.org/10.1002/adfm.201906309;
(d) F. Yan, H. Wu, H. Liu, Z. Deng, H. Liu, W. Duan, X. Liu, H. Zheng, Molecular imaging-guided photothermal/photodynamic therapy against tumor by iRGD-modified indocyanine green nanoparticles, J. Control. Release 224 (2016) 217–228, https://doi.org/10.1016/j.jconrel.2015.12.050;
(e) N. Beziere, N. Lozano, A. Nunes, J. Salichs, D. Queiros, K. Kostarelos, V. Ntziachristos, Dynamic imaging of PEGylated indocyanine green (ICG) liposomes within the tumor microenvironment using multi-spectral optoacoustic tomography (MSOT), Biomaterials 37 (2015) 415–424, https://doi.org/10.1016/j.biomaterials.2014.10.014;
(f) D. Miranda, C. Wan, H.I. Kilian, M.T. Mabrouk, Y. Zhou, H. Jin, J.F. Lovell, Indocyanine green binds to DOTAP liposomes for enhanced optical properties and tumor photoablation, Biomater. Sci. 7 (2019) 3158–3164, https://doi.org/10.1039/C9BM00551J;
(g) I. Noh, M. Kim, J. Kim, D. Lee, D. Oh, J. Kim, C. Kim, S. Jon, Y.-C. Kim, Structure-inherent near-infrared bilayer nanovesicles for use as photoacoustic image-guided chemo-thermotherapy, J. Control. Release 320 (2020) 283–292, https://doi.org/10.1016/j.jconrel.2020.01.032;
(h) C.A. Wood, S. Han, C.S. Kim, Y. Wen, D.R.T. Sampaio, J.T. Harris, K. A. Homan, J.L. Swain, S.Y. Emelianov, A.K. Sood, J.R. Cook, K.V. Sokolov, R. R. Bouchard, Clinically translatable quantitative molecular photoacoustic imaging with liposome-encapsulated ICG J-aggregates, Nat. Commun. 12 (2021) 5410, https://doi.org/10.1038/s41467-021-25452-3;
(i) Q. Chen, J. Chen, M. He, Y. Bai, H. Yan, N. Zeng, F. Liu, S. Wen, L. Song, Z. Sheng, C. Liu, C. Fang, Novel small molecular dye-loaded lipid nanoparticles with efficient near-infrared-II absorption for photoacoustic imaging and photothermal therapy of hepatocellular carcinoma, Biomater. Sci. 7 (2019) 3165–3177, https://doi.org/10.1039/C9BM00528E;
(j) H. Xu, Y. Liu, J. Qu, Z. Yuan, PEGylated liposomal photosensitizers as theranostic agents for dual-modal photoacoustic and fluorescence imaging-guided photodynamic therapy, J. Innov. Opt. Health Sci. 12 (2019), https://doi.org/10.1142/S1793545819410037;
(k) Y. Yan, H. Fu, J. Wang, C. Chen, Q. Wang, Y. Duan, J. Hua, A photo-stable and reversible pH-responsive nano-agent based on the NIR phenazine dye for photoacoustic imaging-guided photothermal therapy, Chem. Commun. 55 (2019) 10940–10943, https://doi.org/10.1039/C9CC05624F;
(l) B. Changalvaie, S. Han, E. Moaseri, F. Scaletti, L. Truong, R. Caplan, A. Cao, R. Bouchard, T.M. Truskett, K.V. Sokolov, K.P. Johnston, Indocyanine green J aggregates in polymersomes for near-infrared photoacoustic imaging, ACS Appl. Mater. Interfaces 11 (2019) 46437–46450, https://doi.org/10.1021/acsami.9b14519;
(m) P. Rong, P. Huang, Z. Liu, J. Lin, A. Jin, Y. Ma, G. Niu, L. Yu, W. Zeng, W. Wang, X. Chen, Protein-based photothermal theranostics for imaging-guided cancer therapy, Nanoscale 7 (2015) 16330–16336, https://doi.org/10.1039/C5NR04428F;
(n) P. Huang, P. Rong, A. Jin, X. Yan, M.G. Zhang, J. Lin, H. Hu, Z. Wang, X. Yue, W. Li, G. Niu, W. Zeng, W. Wang, K. Zhou, X. Chen, Dye-loaded ferritin nanocages for multimodal imaging and photothermal therapy, Adv. Mater. 26 (2014) 6401–6408, https://doi.org/10.1002/adma.201400914.

[94] L. Cheng, K. Yang, Q. Chen, Z. Liu, Organic stealth nanoparticles for highly effective in vivo near-infrared photothermal therapy of cancer, ACS Nano 6 (2012) 5605–5613, https://doi.org/10.1021/nn301539m.

[95] (a) J. Liu, J. Geng, L.-D. Liao, N. Thakor, X. Gao, B. Liu, Conjugated polymer nanoparticles for photoacoustic vascular imaging, Polym. Chem. 5 (2014) 2854–2862, https://doi.org/10.1039/C3PY01587D;
(b) H. Chen, J. Zhang, K. Chang, X. Men, X. Fang, L. Zhou, D. Li, D. Gao, S. Yin, X. Zhang, Z. Yuan, C. Wu, Highly absorbing multispectral near-infrared polymer nanoparticles from one conjugated backbone for photoacoustic imaging and photothermal therapy, Biomaterials 144 (2017) 42–52, https://doi.org/10.1016/j.biomaterials.2017.08.007;
(c) T. Stahl, R. Bofinger, I. Lam, K.J. Fallon, P. Johnson, O. Ogunlade, V. Vassileva, R.B. Pedley, P.C. Beard, H.C. Hailes, H. Bronstein, A.B. Tabor, Tunable semiconducting polymer nanoparticles with INDT-based conjugated polymers for photoacoustic molecular imaging, Bioconjug. Chem. 28 (2017) 1734–1740, https://doi.org/10.1021/acs.bioconjchem.7b00185;
(d) B. Guo, Z. Sheng, K. Kenry, D. Hu, X. Lin, S. Xu, C. Liu, H. Zheng, B. Liu, Biocompatible conjugated polymer nanoparticles for highly efficient photoacoustic imaging of orthotopic brain tumors in the second near-infrared window, Mater. Horiz. 4 (2017) 1151–1156, https://doi.org/10.1039/C7MH00672A;
(e) B. Guo, Z. Sheng, D. Hu, A. Li, S. Xu, P.N. Manghnani, C. Liu, L. Guo, H. Zheng, B. Liu, Molecular Engineering of conjugated polymers for biocompatible organic nanoparticles with highly efficient photoacoustic and photothermal performance in cancer theranostics, ACS Nano 11 (2017) 10124–10134, https://doi.org/10.1021/acsnano.7b04685;
(f) T. Sun, J.-H. Dou, S. Liu, X. Wang, X. Zheng, Y. Wang, J. Pei, Z. Xie, Second near-infrared conjugated polymer nanoparticles for photoacoustic imaging and photothermal therapy, ACS Appl. Mater. Interfaces 10 (2018) 7919–7926, https://doi.org/10.1021/acsami.8b01458;
(g) X. Men, Z. Yuan, Multifunctional conjugated polymer nanoparticles for photoacoustic-based multimodal imaging and cancer photothermal therapy, J. Innov. Opt. Health Sci. 12 (2019), https://doi.org/10.1142/S1793545819300015;
(h) D. Gao, D. Hu, X. Liu, X. Zhang, Z. Yuan, Z. Sheng, H. Zheng, Recent advances in conjugated polymer nanoparticles for NIR-II imaging and therapy, ACS Appl. Polym. Mater. 2 (2020) 4241–4257, https://doi.org/10.1021/acsapm.0c00679;
(i) Y. Miao, C. Gu, B. Yu, Y. Zhu, W. Zou, Y. Shen, H. Cong, Conjugated-polymer-based nanoparticles with efficient NIR-II fluorescent, photoacoustic and photothermal performance, ChemBioChem 20 (2019) 2793–2799, https://doi.org/10.1002/cbic.201900309;
(j) Y. Jiang, P.K. Upputuri, C. Xie, Z. Zeng, A. Sharma, X. Zhen, J. Li, J. Huang, M. Pramanik, K. Pu, Metabolizable semiconducting polymer nanoparticles for second near-infrared photoacoustic imaging, Adv. Mater. 31 (2019), https://doi.org/10.1002/adma.201808166;
(k) T.F. Abelha, P.R. Neumann, J. Holthof, C.A. Dreiss, C. Alexander, M. Green, L.A. Dailey, Low molecular weight PEG–PLGA polymers provide a superior matrix for conjugated polymer nanoparticles in terms of physicochemical properties, biocompatibility and optical/photoacoustic performance, J. Mater. Chem. B 7 (2019) 5115–5124, https://doi.org/10.1039/C9TB00937J;
(l) B. Bao, L. Tong, Y. Xu, J. Zhang, X. Zhai, P. Su, L. Weng, L. Wang, Mussel-inspired functionalization of semiconducting polymer nanoparticles for amplified photoacoustic imaging and photothermal therapy, Nanoscale 11 (2019) 14727–14733, https://doi.org/10.1039/C9NR03490K;
(m) T.F. Abelha, C.A. Dreiss, M.A. Green, L.A. Dailey, Conjugated polymers as nanoparticle probes for fluorescence and photoacoustic imaging, J. Mater. Chem.

B 8 (2020) 592–606, https://doi.org/10.1039/C9TB02582K;
(n) Z. Wei, F. Xin, J. Zhang, M. Wu, T. Qiu, Y. Lan, S. Qiao, X. Liu, J. Liu, Donor–acceptor conjugated polymer-based nanoparticles for highly effective photoacoustic imaging and photothermal therapy in the NIR-II window, Chem. Commun. 56 (2020) 1093–1096, https://doi.org/10.1039/C9CC07821E;
(o) X. Jin, X. Xing, Q. Deng, W. Qing, Z. Liu, Y. Huang, Molecular engineering of diketopyrrolopyrrole-conjugated polymer nanoparticles by chalcogenide variation for photoacoustic imaging guided photothermal therapy, J. Mater. Chem. B 9 (2021) 3153–3160, https://doi.org/10.1039/D1TB00193K.

[96] K. Pu, A.J. Shuhendler, J.V. Jokerst, J. Mei, S.S. Gambhir, Z. Bao, J. Rao, Semiconducting polymer nanoparticles as photoacoustic molecular imaging probes in living mice, Nat. Nanotechnol. 9 (2014) 233–239, https://doi.org/10.1038/nnano.2013.302.

[97] (a) Q. Fan, K. Cheng, X. Hu, X. Ma, R. Zhang, M. Yang, X. Lu, L. Xing, W. Huang, S.S. Gambhir, Z. Cheng, transferring biomarker into molecular probe: melanin nanoparticle as a naturally active platform for multimodality imaging, J. Am. Chem. Soc. 136 (2014) 15185–15194, https://doi.org/10.1021/ja505412p;
(b) A. Liopo, R. Su, A.A. Oraevsky, Melanin nanoparticles as a novel contrast agent for optoacoustic tomography, Photoacoustics 3 (2015) 35–43, https://doi.org/10.1016/j.pacs.2015.02.001;
(c) K.-Y. Ju, J. Kang, J. Pyo, J. Lim, J.H. Chang, J.-K. Lee, pH-Induced aggregated melanin nanoparticles for photoacoustic signal amplification, Nanoscale 8 (2016) 14448–14456, https://doi.org/10.1039/C6NR02294D;
(d) D.L. Longo, R. Stefania, S. Aime, A. Oraevsky, Melanin-based contrast agents for biomedical optoacoustic imaging and theranostic applications, Int. J. Mol. Sci. 18 (2017) 1719, https://doi.org/10.3390/ijms18081719;
(e) D.L. Longo, R. Stefania, C. Callari, F. De Rose, R. Rolle, L. Conti, L. Consolino, F. Arena, S. Aime, Water soluble melanin derivatives for dynamic contrast enhanced photoacoustic imaging of tumor vasculature and response to antiangiogenic therapy, Adv. Healthc. Mater. 6 (2017), https://doi.org/10.1002/adhm.201600550;
(f) B. Fan, X. Yang, X. Li, S. Lv, H. Zhang, J. Sun, L. Li, L. Wang, B. Qu, X. Peng, R. Zhang, Photoacoustic-imaging-guided therapy of functionalized melanin nanoparticles: combination of photothermal ablation and gene therapy against laryngeal squamous cell carcinoma, Nanoscale 11 (2019) 6285–6296, https://doi.org/10.1039/C9NR01122F;
(g) M. Caldas, A.C. Santos, F. Veiga, R. Rebelo, R.L. Reis, V.M. Correlo, Melanin nanoparticles as a promising tool for biomedical applications – a review, Acta Biomater. 105 (2020) 26–43, https://doi.org/10.1016/j.actbio.2020.01.044;
(h) H. Liu, Y. Yang, Y. Liu, J. Pan, J. Wang, F. Man, W. Zhang, G. Liu, Melanin-like nanomaterials for advanced biomedical applications: a versatile platform with extraordinary promise, Adv. Sci. 7 (2020), https://doi.org/10.1002/advs.201903129;
(i) A. Mavridi-Printezi, M. Guernelli, A. Menichetti, M. Montalti, Bio-applications of multifunctional melanin nanoparticles: from nanomedicine to nanocosmetics, Nanomaterials 10 (2020) 2276, https://doi.org/10.3390/nano10112276;
(j) J.-J. Liu, Z. Wang, L.-M. Nie, Y.-Y. Zhu, G. Li, L.-L. Lin, M. Chen, G.-J. Zhang, RGD-functionalised melanin nanoparticles for intraoperative photoacoustic imaging-guided breast cancer surgery, Eur. J. Nucl. Med. Mol. Imaging 49 (2022) 847–860, https://doi.org/10.1007/s00259-021-05545-3;
(k) T. Li, W. Jing, W. Fu, Z. Yan, Y. Ma, X. Li, H. Ji, R. Zhang, Melanin theranostic nanoplatform as an efficient drug delivery system for imaging-guided renal fibrosis therapy, Biomater. Adv. 147 (2023) 213333, https://doi.org/10.1016/j.bioadv.2023.213333.

[98] (a) M. Liu, R. Anderson, X. Lan, P.S. Conti, K. Chen, Recent advances in the development of nanoparticles for multimodality imaging and therapy of cancer, Med. Res. Rev. 40 (2020) 909–930, https://doi.org/10.1002/med.21642;
(b) Y. Xia, C. Xu, X. Zhang, P. Ning, Z. Wang, J. Tian, X. Chen, Liposome-based probes for molecular imaging: from basic research to the bedside, Nanoscale 11 (2019) 5822–5838, https://doi.org/10.1039/C9NR00207C.

[99] L.A. Basal, Y. Yan, Y. Shen, E.M. Haacke, M. Mehrmohammadi, M.J. Allen, Oxidation-responsive, EuII/III-based, multimodal contrast agent for magnetic resonance and photoacoustic imaging, ACS Omega 2 (2017) 800–805, https://doi.org/10.1021/acsomega.6b00514.

[100] M. Devreux, C. Henoumont, F. Dioury, D. Stanicki, S. Boutry, L. Larbanoix, C. Ferroud, R.N. Muller, S. Laurent, Bimodal probe for magnetic resonance imaging and photoacoustic imaging based on a PCTA-derived gadolinium(III) complex and ZW800–1, Eur. J. Inorg. Chem. 2019 (2019) 3354–3365, https://doi.org/10.1002/ejic.201900387.

[101] H. Bai, Y. Wang, Y. Hu, D. Ye, A caspase-3-activatable bimodal probe for photoacoustic and magnetic resonance imaging of tumor apoptosis in vivo, Biosens. Bioelectron. 216 (2022) 114648, https://doi.org/10.1016/j.bios.2022.114648.

[102] (a) F. Chen, L. Teng, C. Lu, C. Zhang, Q. Rong, Y. Zhao, Y. Yang, Y. Wang, G. Song, X. Zhang, Activatable magnetic/photoacoustic nanoplatform for redox-unlocked deep-tissue molecular imaging in vivo via Prussian Blue nanoprobe, Anal. Chem. 92 (2020) 13452–13461, https://doi.org/10.1021/acs.analchem.0c02859;
(b) Y. Li, F. Ye, S. Zhang, W. Ni, L. Wen, H. Qin, Carbon-coated magnetic nanoparticle dedicated to MRI/photoacoustic imaging of tumor in living mice, Front. Bioeng. Biotechnol. 9 (2021), https://doi.org/10.3389/fbioe.2021.800744;
(c) L.-S. Bouchard, M.S. Anwar, G.L. Liu, B. Hann, Z.H. Xie, J.W. Gray, X. Wang, A. Pines, F.F. Chen, Picomolar sensitivity MRI and photoacoustic imaging of cobalt nanoparticles, Proc. Natl. Acad. Sci. 106 (2009) 4085–4089, https://doi.org/10.1073/pnas.0813019106;
(d) Y. Liu, X. Yang, Z. Huang, P. Huang, Y. Zhang, L. Deng, Z. Wang, Z. Zhou, Y. Liu, H. Kalish, N.M. Khachab, X. Chen, Z. Nie, Magneto-plasmonic janus vesicles for magnetic field-enhanced photoacoustic and magnetic resonance imaging of tumors, Angew. Chem. Int. Ed. 55 (2016) 15297–15300, https://doi.org/10.1002/anie.201608338;
(e) Y. Lv, J. Kan, M. Luo, C. Yang, X. Luo, X. Lin, H. Li, X. Li, Y. Li, C. Yang, Y. Liu, X. Li, Multifunctional nanosnowflakes for T1-T2 double-contrast enhanced MRI and PAI guided oxygen self-supplementing effective anti-tumor therapy, Int. J. Nanomedicine 17 (2022) 4619–4638, https://doi.org/10.2147/IJN.S379526;
(f) J. Ren, X. Tang, T. Wang, X. Wei, J. Zhang, L. Lu, Y. Liu, B. Yang, A Dual-modal magnetic resonance/photoacoustic imaging tracer for long-term high-precision tracking and facilitating repair of peripheral nerve injuries, Adv. Healthc. Mater. 11 (2022), https://doi.org/10.1002/adhm.202200183;
(g) C. Yan, D. Liu, L. An, Y. Wang, Q. Tian, J. Lin, S. Yang, Magnetic–photoacoustic dual-mode probe for the visualization of H_2S in colorectal cancer, Anal. Chem. 92 (2020) 8254–8261, https://doi.org/10.1021/acs.analchem.0c00504.

[103] (a) Y. Duan, Y. Xu, D. Mao, W.H. Liew, B. Guo, S. Wang, X. Cai, N. Thakor, K. Yao, C. Zhang, B. Liu, Photoacoustic and magnetic resonance imaging bimodal contrast agent displaying amplified photoacoustic signal, Small 14 (2018), https://doi.org/10.1002/smll.201800652;
(b) J.P. Thawani, A. Amirshaghaghi, L. Yan, J.M. Stein, J. Liu, A. Tsourkas, Photoacoustic-guided surgery with indocyanine green-coated superparamagnetic iron oxide nanoparticle clusters, Small 13 (2017), https://doi.org/10.1002/smll.201701300;
(c) A.A. Bogdanov, A.J. Dixon, S. Gupta, L. Zhang, S. Zheng, M.S. Shazeeb, S. Zhang, A.L. Klibanov, Synthesis and testing of modular dual-modality nanoparticles for magnetic resonance and multispectral photoacoustic imaging, Bioconjug. Chem. 27 (2016) 383–390, https://doi.org/10.1021/acs.bioconjchem.5b00633;
(d) L. Xia, X. Guo, T. Liu, X. Xu, J. Jiang, F. Wang, Z. Cheng, H. Zhu, Z. Yang, Multimodality imaging of naturally active melanin nanoparticles targeting somatostatin receptor subtype 2 in human small-cell lung cancer, Nanoscale 11 (2019) 14400–14409, https://doi.org/10.1039/C9NR04371C;
(e) L. Xia, X. Meng, L. Wen, N. Zhou, T. Liu, X. Xu, F. Wang, Z. Cheng, Z. Yang, H. Zhu, A highly specific multiple enhancement theranostic nanoprobe for PET/MRI/PAI image-guided radioisotope combined photothermal therapy in prostate cancer, Small 17 (2021), https://doi.org/10.1002/smll.202100378;
(f) Y. Liu, N. Kang, J. Lv, Z. Zhou, Q. Zhao, L. Ma, Z. Chen, L. Ren, L. Nie, Deep photoacoustic/luminescence/magnetic resonance multimodal imaging in living subjects using high-efficiency upconversion nanocomposites, Adv. Mater. 28 (2016) 6411–6419, https://doi.org/10.1002/adma.201506460;
(g) M. Poß, R.J. Tower, J. Napp, L.C. Appold, T. Lammers, F. Alves, C.-C. Glüer, S. Boretius, C. Feldmann, Multimodal $[GdO]^{+}[ICG]^{-}$ nanoparticles for optical, photoacoustic, and magnetic resonance imaging, Chem. Mater. 29 (2017) 3547–3554, https://doi.org/10.1021/acs.chemmater.6b05406;
(h) B. Wu, S.-T. Lu, H. Yu, R.-F. Liao, H. Li, B.V. Lucie Zafitatsimo, Y.-S. Li, Y. Zhang, X.-L. Zhu, H.-G. Liu, H.-B. Xu, S.-W. Huang, Z. Cheng, Gadolinium-chelate functionalized bismuth nanotheranostic agent for in vivo MRI/CT/PAI imaging-guided photothermal cancer therapy, Biomaterials 159 (2018) 37–47, https://doi.org/10.1016/j.biomaterials.2017.12.022;
(i) C. Gosée, J. Moreau, C. Cadiou, M. Callewaert, C. Henoumont, L. Larbanoix, M. Molinari, S.N. Voicu, C. Portefaix, S. Laurent, F. Chuburu, Multimodal nanogels combining ZW800-1 as an optical absorber and gadolinium chelates for multispectral optoacoustic tomography (MSOT) and magnetic resonance, 2025;
(j) J.E. Lemaster, Z. Wang, A. Hariri, F. Chen, Z. Hu, Y. Huang, C.V. Barback, R. Cochran, N.C. Gianneschi, J.V. Jokerst, Gadolinium doping enhances the photoacoustic signal of synthetic melanin nanoparticles: a dual modality contrast agent for stem cell imaging, Chem. Mater. 31 (2019) 251–259, https://doi.org/10.1021/acs.chemmater.8b04333.

[104] (a) G.L. Griffiths, C. Vasquez, F. Escorcia, J. Clanton, L. Lindenberg, E. Mena, P. L. Choyke, Translating a radiolabeled imaging agent to the clinic, Adv. Drug Deliv. Rev. 181 (2022) 114086, https://doi.org/10.1016/j.addr.2021.114086;
(b) E. Blanco, H. Shen, M. Ferrari, Principles of nanoparticle design for overcoming biological barriers to drug delivery, Nat. Biotechnol. 33 (2015) 941–951, https://doi.org/10.1038/nbt.3330;
(c) N. Desai, Challenges in development of nanoparticle-based therapeutics, AAPS J. 14 (2012) 282–295, https://doi.org/10.1208/s12248-012-9339-4;
(d) L.A. Lane, X. Qian, A.M. Smith, S. Nie, Physical chemistry of nanomedicine:

understanding the complex behaviors of nanoparticles *in vivo*, Annu. Rev. Phys. Chem. 66 (2015) 521–547, https://doi.org/10.1146/annurev-physchem-040513-103718;
(e) S.Y. Fam, C.F. Chee, C.Y. Yong, K.L. Ho, A.R. Mariatulqabtiah, W.S. Tan, Stealth coating of nanoparticles in drug-delivery systems, Nanomaterials 10 (2020) 787, https://doi.org/10.3390/nano10040787;
(f) S. Schöttler, G. Becker, S. Winzen, T. Steinbach, K. Mohr, K. Landfester, V. Mailänder, F.R. Wurm, Protein adsorption is required for stealth effect of poly (ethylene glycol)- and poly(phosphoester)-coated nanocarriers, Nat. Nanotechnol. 11 (2016) 372–377, https://doi.org/10.1038/NNANO.2015.330;
(g)A. Erfani, J. Seaberg, C. P. Aichele, J. D. Ramsey, Interactions between biomolecules and zwitterionic moieties: a review, Biomacromolecules 21 (2020) 2557−2573. doi:https://doi.org/10.1021/acs.biomac.0c00497. (h) S.M. Gheibi Hayat, V. Bianconi, M. Pirro, A. Sahebkar, Stealth functionalization of biomaterials and nanoparticles by CD47 mimicry, Int. J. Pharm. 569 (2019) 118628, https://doi.org/10.1016/j.ijpharm.2019.118628;
(i) J. Li, T. Wu, S. Li, X. Chen, Z. Deng, Y. Huang, Nanoparticles for cancer therapy: a review of influencing factors and evaluation methods for biosafety, Clin. Transl. Oncol. 25 (2023) 2043–2055, https://doi.org/10.1007/s12094-023-03117-5.